Advanced Materials Technologies

ADVANCED MATERIALS TECHNOLOGIES
www.advmattechnol.com

REVIEW OPEN ACCESS

Fabrication Technologies for Soft, Multimaterial Optical Fibers for In Vivo Diagnostics and Phototherapy, With a Focus on Extrusion Printing

Zahra Kafrashian[1,2] | Jun Feng[1] | Aránzazu del Campo[1,2]

[1]INM – Leibniz Institute for New Materials, Saarbrücken, Germany | [2]Chemistry Department, Saarland University, Saarbrücken, Germany

Correspondence: Aránzazu del Campo (aranzazu.delcampo@leibniz-inm.de)

Received: 25 August 2025 | **Revised:** 29 December 2025 | **Accepted:** 11 January 2026

Keywords: extrusion printing | multimaterial | optical fiber | photo diagnostics and therapy | soft

ABSTRACT

Multimaterial optical fibers provide a versatile platform for integrating diverse functionalities—such as waveguiding, side emission, sensing, and actuation—into a single filament. Although traditional multimaterial fibers have primarily been fabricated from rigid materials such as silica and thermoplastics for optoelectronic applications, recent developments have shifted the focus toward soft systems composed of elastomers, hydrogels, and their composites. Owing to their mechanical compliance and biocompatibility, these soft fibers are particularly well suited for wearable, implantable, and tissue-integrated devices used in diagnostics and phototherapy. This review provides a comprehensive overview of the rapidly developing field of soft multimaterial optical fibers, highlighting key material combinations and fabrication strategies that enable multifunctional performance. Particular emphasis is placed on extrusion-based multimaterial printing—including coaxial and segmented extrusion—which has significantly expanded the architectural and functional design space of soft optical fibers. Remaining challenges, including material compatibility, interfacial and surface quality, and printing resolution, are critically discussed. Finally, the review outlines emerging opportunities for advancing these fabrication approaches toward practical and clinically relevant biomedical applications.

1 | Introduction

Light exposure can be used for non-invasive and local exploration (diagnostics) or treatment (phototherapy) of diseased sites inside the body [1–4]. Light offers high spatial and temporal resolution, as well as orthogonality to surrounding biological and biochemical processes within practicable wavelengths and dose ranges. However, the interaction of light with tissue via absorption, scattering and reflection limits the propagation of light inside the body to a few millimeters and constrains the current application of light-based approaches in medicine to superficial sites (skin wearables), or to temporal treatments through endoscopic devices that can bring the light source to the application site.

To extend the temporal window of the diagnostics and the spatial window of the therapeutic applications, implanted light sources (e.g. LEDs) and implanted optical fibers connected to an external light source are used to deliver light inside the body [5]. Due to their low material content and large surface-to-volume ratio, optical fibers are preferred when the application site has a difficult geometry or when large tissue volume needs to be illuminated. In addition, optical fibers can integrate additional functionalities

Zahra Kafrashian and Jun Feng contributed equally to this work.

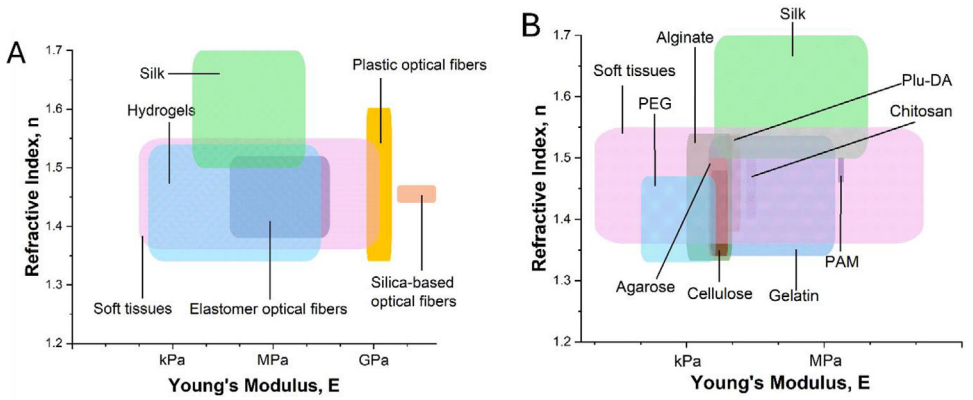

FIGURE 1 | (A) The comparison of the optical materials across the mechanical properties and refractive index. (B) The comparison of the hydrogel optical materials across the mechanical properties and refractive index. The figure was plotted based on previous reports [8, 9, 13, 28, 51, 54–76].

beyond light transport and serve for optical reading and to sense changes at the application site.

Rigid optical fibers based on silica glass, polycarbonates, polyimides or polyacrylates have been explored as optical fibers in in vivo contexts [6, 7]. Nevertheless, their mechanical stiffness creates a pronounced mismatch with surrounding soft tissues, compromising biocompatibility and often inducing inflammation or fibrosis. In contrast, Soft elastomeric and hydrogel-based optical fibers offer a more biocompatible alternative to conventional rigid fibers because their mechanical properties closely match those of biological tissues (Young's modulus of soft tissues typically ranges from a few Pa to several hundred MPa [8]) (Figure 1). These materials also meet the optical performance requirements for biomedical light delivery, where relevant distances range from 1 mm to 1 m and correspond to acceptable optical losses of approximately 43–0.43 dB/cm [9]. Soft optical fibers, with reported optical losses of 0.1–28 dB/cm [9–16], therefore satisfy the fundamental criteria for application in vivo.

The growing body of demonstrations underscores the versatility of soft optical fibers in biomedical contexts. Demonstrations of soft optical fibers in in vivo applications include:

- *Photodynamic therapy* with light-emitting fabrics made from woven side-emitting polymeric optical fibers to treat skin conditions like actinic keratosis when integrated into a helmet [17]. Arrays of hydrogel microneedles have also been applied to deliver light and photosynthesizer transdermally [18].
- *Tissue crosslinking* using a flexible elastomeric polyurethane/polydimethylsiloxane (PU/PDMS) optical waveguide to deliver blue light to the equatorial sclera. A 2-fold increase in scleral stiffness was realized by photocrosslinking [19].
- *Photobiomodulation* or pain relief using low-intensity red or near-infrared light with side-emitting polymer fibers incorporated in wearable devices for large-area exposure [20, 21].
- *Photothermal therapy* with an optical fiber inserted in a needle to guide it into the tumor and used as reservoir for the photothermal agent [22].
- *Optogenetics* with hydrogel patches or fibers to deliver light to activate cells for light-controlled therapy or modulate the animal's behavior [11, 23].

In the field of diagnostics [24], implantable hydrogel waveguides carrying fluorescent and luminescent probes (i.e. antibody-conjugated organic dyes for detecting proteins and biomarkers, glucose [25, 26] or blood oxygen [27, 28], dye-linked nucleic acids for monitoring gene expression, pH-sensitive fluorophores, or Förster resonance energy transfer-based sensors [29]) have allowed in vivo monitoring of proteins, peptides, RNA, electrolytes, biomarkers, and toxic substances. For example, *P*oly(acrylamide-co-poly(ethylene glycol) diacrylate) hydrogel waveguides with an alginate hydrogel cladding layer functionalized with glucose-specific receptors were used to monitor glucose levels in porcine tissue by measuring the variation in light transmission through the hydrogel fibers [30]. In similar manner, wearable devices can integrate sensing optical fibers woven into textiles to detect different kinds of biomolecules [31].

The implementation of these technologies relies on fabrication routes that can produce compliant, optically transparent filaments with defined architectures. To fabricate soft optical fibers, thermal drawing, extrusion and molding based processes have been applied. To increase functionalities beyond light guiding, such as electrical or mechanical sensing, filament fabrication technologies have been adapted to process fibers with coaxial layers of different materials, for example using multimaterial preforms in thermal drawing, or adding coating steps in molding processes [28, 32–38]. The recent development of multimaterial printing heads and printable inks for biomedical applications have significantly expanded the possibilities to process multimaterial filaments by extrusion, many of them also applicable to process soft optical fibers. For example, multi-shell filaments have been co-extruded using inks of different properties and coaxial nozzles [39], Janus filaments using single Y or V-shaped nozzles with multiple inlets [40], multicore filaments using microfluidics printing heads [41], and more recently filaments with helicoidal cores using rotational printing heads [42]. In coaxial extrusion printing, processing conditions (temperature, pressure) and material flow properties can be combined synergistically to flexibly tune the dimensions and structure of the filament as it is

extruded. More recently, the possibility to vary the compositions and material's properties along the filament has been realized. Filaments with gradient composition using mixing nozzles [43] or multimaterial segmented filaments by switching the flow between inlets of a single nozzle [44–46] have been reported from photocurable silicones and thermo-reversible hydrogels as inks. In this review we present the current status of multimaterial filament fabrication with a focus on materials and methodologies which have been or could be transferred to the fabrication of multifunctional soft optical fibers, in particular extrusion printing technologies.

2 | Fundamental Properties of Materials for Soft Optical Fibers

2.1 | Optical Properties

Optical waveguides guide light over long distances with minimal loss based on total internal reflection, which occurs when the refractive index of the waveguiding medium (typically the fiber core) exceeds that of the surrounding medium (typically the fiber cladding) [47]. The *optical loss*, also referred to as optical attenuation, describes the reduction in light power or signal strength as it propagates through a waveguide and is typically measured in decibels per centimeter (dB/cm). Optical loss in soft materials can be divided into two primary categories: intrinsic loss and extrinsic loss [48]. Both mechanisms are influenced by the inherent material properties and the structure of the waveguide.

Intrinsic optical loss is associated with the material's inherent absorption and scattering properties [49]. This loss can arise from (i) absorption due to electronic transitions, which are typically in the Visible Light (VIS) or Ultraviolet (UV) ranges for organic molecules; (ii) absorption due to molecular vibrations in the Near-Infrared (NIR) range; (iii) light scattering due to the inherent structural heterogeneity of polymer networks, which have comparable sizes (nm to micrometer scale) to the wavelength of light (Mie scattering). Extrinsic loss arises from defects such as surface roughness, structural imperfections, or the inclusion of impurities (dust particles, bubbles) [49]. These external factors cause additional scattering and absorption, further reducing the efficiency of the optical waveguide.

In soft biomedical waveguides, attenuation values from 0.1 to 25 dB/cm are common in VIS-NIR range [9]. For context, silica-based optical fibers, widely used in telecommunications, exhibit far lower attenuation (0.2 dB/km at 1550 nm) [50]. Hard polymer-based waveguides exhibit higher attenuation than silica, i.e. poly (methyl methacrylate) fibers show attenuation values of 55 dB/km at 538 nm and polycarbonate fibers 600 dB/km at 670 nm [51].

The refractive index (RI) of a material indicates the extent to which light of a particular wavelength slows down as it passes through the material. It depends on the packing density (free volume), the polarizability, and the difference between the wavelength of the light and the material's maximum absorption wavelength [49, 52]. At optical frequencies, electronic polarization is the dominant contributor to RI. Aromatic polymers have higher RI than aliphatic ones due to better packing and higher electronic polarizability. Densification increases the RI. In hydrogel optical fibers, the increase in the polymer content increases RI. For example, poly(ethylene glycol) diacrylate (PEGDA) hydrogels showed RI ranging from 1.36 to 1.46 when the polymer concentration changed from 20 to 70 wt.% [53].

2.2 | Mechanical Properties

A mechanical mismatch between implanted devices and surrounding tissues can induce stress concentrations that may damage adjacent healthy tissue. To minimize such adverse effects, the mechanical properties of implantable waveguides should closely approximate those of the host environment. Soft optical fibers improve mechanical conformability and enable intimate integration with soft, curved, or dynamically moving tissues [9]. Their compliance reduces foreign-body responses and allows stable optical performance during physiological deformation.

Reported waveguiding materials exhibit a wide range of mechanical behaviors, reflecting the diversity of systems used for soft and rigid optical fibers. Figure 1A compares commonly used optical fiber materials according to their Young's modulus and refractive index, highlighting the distinct mechanical and optical domains occupied by soft tissues, hydrogels, elastomer-based fibers, plastic optical fibers, and silica fibers. Soft tissue and hydrogel materials fall within the low-modulus regime (kPa–MPa) and exhibit refractive indices of approximately 1.33–1.55 [8, 9, 54, 55], whereas plastic and silica fibers span substantially higher moduli (MPa–GPa) [51] and higher refractive indices (1.34-1.59).

Figure 1B presents representative hydrogel systems used in soft optical fibers—including agarose, cellulose, gelatin, poly(ethylene glycol) (PEG), polyacrylamide (PAM), alginate, chitosan, Pluronic F127 diacrylate (Plu-DA), and silk—illustrating their broad tunability and the extent to which their properties overlap with those of soft biological tissues. This overlap underscores the suitability of hydrogel-based fibers for in vivo diagnostics and therapeutic light delivery.

For example, natural polymers like regenerated silk fibroin (SF) hydrogels have mechanical properties similar to cartilage, skin, and the eye's lens, with a tunable modulus ranging from 0.07 to 6.5 MPa, comparable to soft tissues [58, 76]. For soft and stretchable waveguides, elastomers derived from PU [19], polysiloxanes [77], or citrate-based polyesters have been used [78]. PDMS is commonly used due to its good biocompatibility, ability to be molded at sub-micron scales, oxygen permeability, and chemical inertness [79]. PDMS's high optical transparency across the visible spectrum makes it an attractive option for stretchable waveguides [80]. Tailoring the crosslinking density of PDMS allows for core-cladding waveguide designs with customizable RI. [81, 82]

Hydrogel-based waveguides represent softer alternatives with mechanical properties close to soft tissues. These hydrogels

can be formed through either chemical or physical crosslinking. More complex network architectures like interpenetrating polymer networks can enhance hydrogel's strength, extensibility and toughness without drastically increasing stiffness [83], making hydrogels an appealing choice for soft tissue-compatible waveguides.

3 | Material Combinations that can add Functionalities (Beyond Waveguiding) to Hybrid, Soft Optical Fibers

Hydrogels, elastomers and thermoplastics have been used for fabricating soft optical waveguides. Hydrogels are capable of retaining substantial amounts of water and can be responsive to external stimuli under physiological conditions. They exhibit adjustable optical properties (transparence and RI) and tunable mechanical properties. These features make hydrogels well-suited for soft optical waveguides to be applied in the body [9, 11, 23, 25, 28, 30, 53, 84–98]. Elastomers [19, 77, 78, 80, 99–108], either of natural or synthetic origin, can undergo significant elastic deformation under tensile and compressive stress. For example, PDMS is an attractive option for stretchable waveguides due to its good biocompatibility, oxygen permeability, chemical inertness and high optical transparency [79, 80]. Thermoplastics, such as polylactic acid (PLA) [109–112], polydioxanone [113], and polyethersulfone [114], have also been used to fabricate optical waveguides due to their good biocompatibility, despite their inherently rigid mechanical properties. Degradable soft thermoplastic materials for optical waveguides are PLA and its copolymers (with glycolic acid or caprolactone), which show glass transition temperatures below body temperature [115]. Naturally derived polymers such as silk [38, 116–123], chitosan [124, 125], agarose [65], gelatin [66, 69], and cellulose [126–129], alginate [130, 131] have shown potential as materials for soft optical waveguides. These materials are biodegradable and can be absorbed by the body [132].

The primary function of soft optical waveguides is to deliver light remotely to a specific target location. By incorporating dye molecules, nanoparticles, quantum dots, stimuli-responsive components or even living cells into the waveguiding material, *hybrid optical fibers* with expanded functionalities can be created, like sensing capability or active response. For instance, the integration of fluorescent dyes in soft PDMS optical waveguides allows for motion detection [104]. Up-conversion nanoparticles [77], gold nanoparticles [28, 93], and metal–organic frameworks [96] have been integrated into elastomeric or hydrogel waveguides for temperature sensing, blood oxygenation monitoring, and fluorescence-based detection. By incorporating quantum dots [90, 91, 95], into PEGDA hydrogel optical waveguides have been utilized for detecting heavy metal ions. Additionally, modifying hydrogel precursors with glucose-responsive monomers enables the fabrication of hydrogel optical waveguides for glucose monitoring [25, 30]. With their excellent biocompatibility, hydrogel optical waveguides have also been used to encapsulate optogenetically engineered cells, facilitating light-controlled therapy and real-time monitoring of systemic cellular toxicity caused by quantum dots [11].

4 | Fabrication Technologies to Process Soft Multimaterial Optical Fibers

Optical fibers can be fabricated by thermal drawing, molding, spinning and extrusion printing (Figure 2). All these methods support the processing of multiple materials within a single fiber, either in coaxial or segmented geometries. The methods differ in terms of flexibility, scalability, and the range of achievable designs. In the following section, we describe how these technologies have been extended from fabricating monocomponent to multimaterial soft optical fibers.

Among these methods, extrusion printing has recently developed and is a major focus of this review article. Extrusion printing offers unique advantages, including: 1) Capability to geometric and structural complexity to create custom cross-sections, embedded channels, or spatially varied structures such as graded-index profiles and segmented cores [133]. 2) Multimaterial integration possibility, by allowing precise placement of different materials within a single fiber, enabling core–cladding architectures with tailored RI or segmented fibers incorporating functional additives [134]. 3) Rapid prototyping and customization through continuous design–test–optimize cycles, and facilitation of the development of fiber geometries with novel functions. Extrusion printing supports both continuous and on-demand, small-batch production, which is particularly valuable for research and biomedical applications [133].

4.1 | Soft Multimaterial Optical Fibers by Thermal Drawing

Thermal drawing is a technique used to fabricate fibers from thermoplastic polymers, which can be divided into direct and indirect thermal drawing (Figure 2A). Direct thermal drawing is used to produce monocomponent fibers from the polymer melt. For example, poly(L-lactic acid) (PLLA) has been thermally melted and drawn into fibers using glass capillary tubes, followed by cooling to induce a crystalline-to-amorphous phase transition. The fiber diameter can be controlled by adjusting the drawing speed. The resulting fibers exhibit high mechanical flexibility (bending stiffness $\approx 1.5 \times 10^4$ N/m) and good optical transparency, with losses of 1.64 dB/cm in air and 1.87 dB/cm in water at 473 nm [112]. These PLLA fibers have been employed for intracranial light delivery and detection, enabling deep-brain fluorescence sensing and in vivo optogenetic interrogation. A similar approach has been used to fabricate PDMS optical fibers. In this case, a partially cured PDMS rod was drawn to fibers with lengths of several tens of centimeters with an optical loss of 0.5 dB/cm at 632 nm [135].

In indirect thermal drawing, the process starts from a fiber preform, which is a larger-scale version of the desired fiber with typically more than 100 times the final diameter (Figure 2A right). This preform is heated at temperatures well above the glass transition temperature (Tg), when it becomes soft and pliable, and is drawn to a thin fiber. The resulting fibers have diameters of hundreds of microns depending on the drawing temperature and speed and can be drawn to diameters below tens of microns through a second drawing step. Once the desired dimensions are

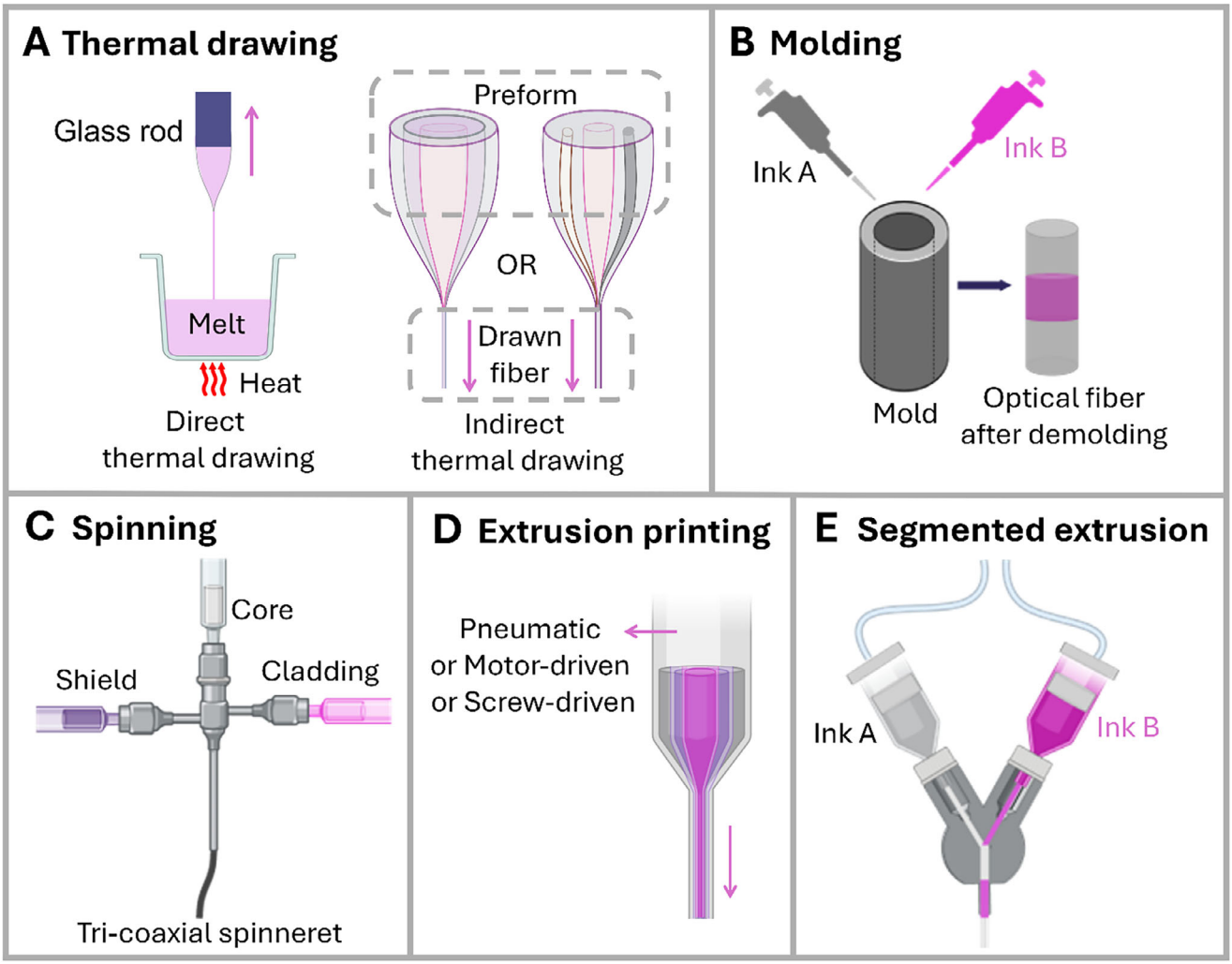

FIGURE 2 | Schematic illustration of different fabrication technologies to process soft multimaterial optical fibers by: (A) thermal drawing, (B) molding, (C) spinning, (D) extrusion printing and (E) segmented extrusion. Created with BioRender.com.

reached, the fiber is cooled below Tg to solidify in its final shape. Controlled heating and precise drawing conditions are essential to draw fibers with constant dimensions and optical properties.

Indirect thermal drawing allows the integration of additional functionalities into a fiber's cladding by using preforms with a layered, multi-material structure [32]. For instance, incorporating metal layers can provide electrical and thermal conductivity, enabling functions such as signal transmission and heating. Similarly, integrating semiconductor layers can introduce optoelectronic properties, allowing for light detection and emission. This method has been applied in the fabrication of soft core-cladding and multi-material fibers [33, 136, 137]. Preforms composed of soft thermoplastic elastomers—such as poly(styrene-b-(ethylene-co-butylene)-b-styrene) (SEBS) or Geniomer—combined with polymeric optical guides, metallic wires, and microfluidic channels have been thermally drawn into fibers [33]. These fibers had a diameter of around 700 μm and were produced at temperatures ranging from 200 to 250 °C, with drawing speeds between 100 and 900 mm/min. Fibers with hollow channels of 100 μm in diameter have also been drawn, offering potential for use as microfluidic conduits for fluid sampling or delivery. We highlight that research on the use of thermal drawing for fabricating multimaterial optical fibers has been extensively reviewed elsewhere [34–37] and is not the focus of this article.

Indirect thermal drawing requires using materials with similar rheological properties and can withstand the thermal and mechanical stresses of the process without degrading or losing their optical properties. This can potentially limit the application of this technology to multimaterial fabrication.

4.2 | Soft Multimaterial Optical Fibers by Molding

Molding represents one of the earliest and most straightforward approaches for fabricating soft optical fibers. In this method, a liquid precursor of the optical material is injected or cast into a mold of predetermined geometry, then solidified through thermal curing, photopolymerization, or physical gelation to form a freestanding waveguide (Figure 2B). The mold can be made from glass capillaries, flexible tubing, or 3D-printed templates that define the fiber diameter and cross-sectional profile. Depending on the mold and material viscosity, fiber diameters typically range from hundreds of micrometers to several millimeters.

Thermoset and thermoplastic elastomers such as PDMS, PU, PLLA, and citrate-based polyesters have been widely molded to produce transparent and flexible optical fibers. [12, 19, 78, 103, 109, 138]. In these systems, curing temperature and crosslinking kinetics strongly affect optical clarity and refractive-index uniformity. For example, PDMS fibers molded at 60–80°C with controlled curing rates yield optical losses below 0.3 dB/cm at 450 nm, while fast curing or bubble entrapment increases scattering and attenuation [82]. Biodegradable PLLA and PU waveguides have shown refractive indices around 1.45–1.49, allowing for numerical apertures (NAs) ≈0.2–0.3 when paired with lower-index claddings, suitable for coupling light from LEDs or laser diodes in implantable systems.

Molding is also effective for hydrogel-based fibers, where aqueous precursors such as PEGDA, PAM, agarose, or silk fibroin are crosslinked inside tubing or channel molds [11, 38, 65, 92]. Hydrogel waveguides typically exhibit diameters of 500 μm – 1 mm and optical losses of 0.1–25.0 dB/cm depending on water content and network homogeneity [9, 16]. Because these materials possess refractive indices in the range 1.34–1.50 [9], they are particularly suitable for biological environments where index matching minimizes reflection losses.

Molding is inherently a batch-based process, meaning that the fabrication of multimaterial fibers with multiple functional layers often requires several sequential molding [38] or post-coating [28] steps. Each additional step demands precise alignment and strong interfacial bonding to preserve core–cladding adhesion, which is crucial for maintaining modal stability and transmission efficiency [139, 140]. Future developments in soft mold materials and automated demolding systems may help transform this technique into a continuous or hybrid molding–extrusion process, enabling the production of multimaterial optical fibers with finely controlled geometries and enhanced optical performance [141–143].

4.3 | Soft Multimaterial Optical Fibers by Spinning

In a spinning process, the precursor materials, typically a polymer solution, are extruded through a spinneret into a clogging bath, where they eventually form thin and continuous filament (Figure 2C). Using wet-jet spinning, core-cladding optical fibers from cellulose (higher RI) and cellulose acetate (lower RI) solutions were fabricated in a two-step process. First, regenerated cellulose core was processed by dry–wet spinning a 5 wt.% cellulose solution in 1-ethyl-3-methylimidazolium acetate into a water bath (coagulant). Next, a filament coater was used to apply a cladding layer from a 50 wt.% solution of cellulose acetate in acetone. Fibers with diameter of 210 μm including a cladding thickness of 3.40 ± 0.20 μm were obtained and showed a minimum attenuation of 5.9 dB/cm at 1130 nm and optical losses <10 dB/cm in the 750–1350 nm range [64].

Core–cladding fibers with variable RI (step- and gradient-index hydrogel fibers) were obtained by wet-spinning a 7% alginate solution through a microfluidic tube into a 0.1 M $CaCl_2$ bath, followed by dip-coating in different alginate or gellan gum solutions, which were crosslinked by 0.1 M $CaCl_2$ [144]. The hydrogel fibers were able to modulate optical signals in response to mechanical stimuli. By incorporating plasmonic nanoparticles in the core, the fibers were used for molecular detection.

Tough optical waveguides from mineralized silk were obtained by spinning a 15 wt.% mixture of SF and $CaCO_3$ nanocrystals (NCs) in water [145]. The SF chains were used as the guide agent and template for the formation and growth of $CaCO_3$ NCs. $CaCO_3$ NCs within the regenerated SF network served as nucleation templates for mineralization during the spinning, The mineralized silk fibers with optical loss of 0.46 dB/cm at 808 nm showed a tensile strength of 0.83 ± 0.15 GPa and toughness of 181.98 ± 52.42 $MJ \cdot m^{-3}$. Using a microfluidic chip that mimicked the spider's major ampullate gland, optical fibers of regenerated SF and cellulose nanofibers were fabricated by wet spinning [146]. The hybrid fibers exhibited an optical loss of 1.0 dB/cm at 650 nm and a strength at failure of 710 ± 33 MPa, higher than natural silk fibers.

Although spinning—including wet, dry–wet, and wet-jet spinning—provides a versatile route for producing continuous polymer filaments, several limitations constrain its use for soft optical fiber fabrication. Spinning generally requires multistep workflows such as core formation, coagulation, post-coating, and solvent exchange [147, 148], which increase processing complexity and make it challenging to maintain core–cladding concentricity and interfacial quality. These issues become more pronounced with hydrophobic or elastomeric polymers. For example, in one approach, a PDMS core jet is formed within a temporary alginate shell in a microfluidic coaxial setup. The composite filament is stabilized as the alginate crosslinks in a $CaCl_2$ bath while the PDMS cures, after which the alginate is removed in concentrated NaCl to yield continuous PDMS fibers [149]. Wet and dry–wet spinning rely on heat or solvent exchange, leading to slow diffusion, long processing times, and risks of defects or residual solvent that reduce optical clarity or biocompatibility [150]. In another report, AIEgen-doped PDMS was partially cured and extruded into a 170–180°C oil bath, requiring strict temperature uniformity to avoid deformation during the rapid (~3 s) curing stage [151]. More broadly, spinning's dependence on fluid flow, coagulation kinetics, and diffusion-controlled solidification makes precise control of cladding thickness and core uniformity difficult, affecting optical loss and modal stability.

4.4 | Soft Multimaterial Optical Fibers by Extrusion Printing

In an extrusion process, the polymer is forced to flow through an extrusion head (nozzle) to produce fibers with a specific cross-sectional profile. Extrusion allows for the continuous production of fibers with appropriate context. Either thermoplastic polymers can be extruded at temperatures above their flow temperature and cooled right after to retain the form, or liquid reactive precursor mixtures with appropriate rheological properties can be extruded and crosslinked after the extrusion process to retain the shape of the nozzle. For example, aqueous SF solutions (28–30 wt.%) were extruded into fiber geometry using a 5 μm glass nozzle. Solidification of the fiber was achieved by direct extrusion into a methanol-rich reservoir. Methanol induces a structural transition in the SF, from amorphous random coil to rigid β-sheet

conformation and stabilizes the extruded waveguides. Fibers with a diameter of 5 μm and several centimeters in length were produced [116]. These waveguides exhibited an attenuation of 0.25 dB/cm at 633 nm. In our previous work, soft optical fibers were extruded from degradable thermoplastic polyesters [115]. Melted poly(D,L-lactide) and its copolymers were extruded at temperatures between 90 and 100°C to produce optical waveguides. These polymers have glass transition temperatures between 16 and 38°C and, therefore, are soft solids at body temperature. The resulting fibers exhibited optical losses ranging from 0.02 to 0.26 dB/cm in air and 0.14 to 0.44 dB/cm in tissue. These fibers were capable of delivering near-UV visible light (405 nm) through ≥8 cm of tissue, successfully activating photocleavage reactions in 3D cell cultures. In the following sections, different extrusion printing methods to extrude multimaterial fibers are described.

4.4.1 | Coaxial Extrusion Printing of Multimaterial Fibers

Multi-material coaxial printing enables the simultaneous extrusion of fibers containing different materials through a single nozzle. Using a coaxial nozzle (Figure 2D), materials with various properties can be aligned and deposited in a concentric configuration as part of a single fiber. Unlike layer-by-layer coating processes, coaxial multimaterial printing enables one-step integration of multiple functional materials within the single printed filament. To enable successful coaxial printing, the materials used must meet several fundamental requirements: viscosity compatibility to ensure uniform flow, shear-thinning behavior for smooth extrusion, rapid gelation or crosslinking to maintain the printed structure, chemical compatibility to avoid adverse reactions at the interfaces such as precipitation or degradation, interfacial stability to ensure good adhesion or limited diffusion between layers, and solvent compatibility—meaning the materials should use the same or miscible solvents to prevent phase separation during extrusion. By coupling the extrusion nozzle to a printing head, the 1D device architecture can be printed to customizable 2D and 3D shapes.

Coaxial extrusion for the continuous fabrication of soft optical fibers in planar and nonplanar configurations was first demonstrated using a photocurable hybrid organic–inorganic core fluid (OrmoClear, Micro Resist Technology) as core material and a fugitive material (35 wt.% of Pluronic F127 in water) for the shell [154]. The resulting fibers exhibited an optical loss of approximately 0.1 $dB \cdot cm^{-1}$ at 633 nm. Even though the final soft optical fiber retained only the core material, the study demonstrated the possibility of fabricating multimaterial fibers by coaxial extrusion.

Subsequent studies expanded the method to a wide range of material systems. Using a coaxial nozzle (Figure 3A), trilayer optical fibers with different optical properties in each layer were printed [144]. The core ink contained a 2 wt.% alginate solution with living cells, the intermediate cladding layer contained 0.5 wt.% gellan gum for light confinement, and the outer shield layer was composed of 1.0 wt.% gellan gum to provide mechanical stability. The resulting core–cladding–shield filaments had a diameter of approximately 1.5 mm and supported light transmission along an internal waveguiding channel for lengths exceeding 20 cm. The waveguiding core was used to detect the changes in the cell population (growth or secretion of fluorescent or coloured metabolites), enabling real-time monitoring of cell proliferation and drug response. This approach demonstrates the potential of using light transmission changes to quantify complex biological processes.

In our previous work, we used coaxial extrusion-based printing combined with in situ photopolymerization to fabricate core–cladding step-index optical fibers from hydrogels [53] and elastomeric materials [13]. The hydrogel waveguides featured a core made of an 80 wt.% solution of dithiothreitol-modified polyethylene glycol diacrylate (PEGDA-DTT), with diameters ranging from 340 to 640 μm, and a cladding layer composed of 33 wt.% Plu-DA, with a fixed outer diameter of 1.02 mm. Plu-DA formed a physical hydrogel with shear-thinning properties, allowing it to behave like a paste that could be easily extruded. This cladding provided structural support for the liquid PEGDA-DTT core during printing. The resulting core–cladding hydrogel fibers exhibited optical losses of less than 0.2 dB/cm at 405 nm [53]. Using the same approach, we also printed elastomer-based fibers consisting of a photocrosslinkable PDMS core and a Plu-DA cladding (Figure 3B) [13]. These fibers had core diameters between 100 and 550 μm and the same fixed outer diameter of 1.02 mm. Continuous fibers up to 50 cm in length were readily produced. They showed optical losses ranging from 0.13 to 0.34 dB/cm in both air and tissue environments across the 405–520 nm wavelength range. Notably, the elastic fibers could be stretched to more than five times their original length. Both types of printed waveguides have a Young's Modulus (Plu-DA cladding) of 150 kPa and were effective in transmitting light through more than 5 centimeters of muscle tissue and successfully activated photochemical and optogenetic responses under conditions that closely mimic physiological environments [13, 53].

In addition to the examples mentioned above, more advanced coaxial printing technologies have been developed. Although these methods have not yet been applied to the fabrication of soft optical fibers, it is worthwhile summarizing them, as they offer design concepts with significant potential for adoption by the soft optical fiber community.

Using a 4-layer tapered coaxial nozzle, soft multi-core-shell fibers were fabricated (Figure 3C) [152]. The nozzle featured a 200 μm diameter inner core and three cladding layers, each 200 μm thick. The fiber consisted of a conductive core made of thermoplastic PU containing silver flakes, a first cladding layer of reactive silicone with embedded ZnS particles (ZnS/DS), a second cladding layer composed of polyvinyl alcohol (PVA), polyethylene oxide (PEO) and lithium chloride (LiCl), and an outer cladding layer of reactive silicone. Fiber-shaped electroluminescent devices were fabricated by simultaneous printing of the electrode, phosphor, and encapsulation inks. These fibers offered customized complex arbitrary shape and high stretchability and have potential for application in textile-based and body-mounted optoelectronic devices. Using a similar fabrication approach, multicore–shell capacitive fibers were printed with a custom-designed, four-nozzle coaxial printhead [155]. The fibers comprise an inner conductive core (335 ± 6 μm), a dielectric

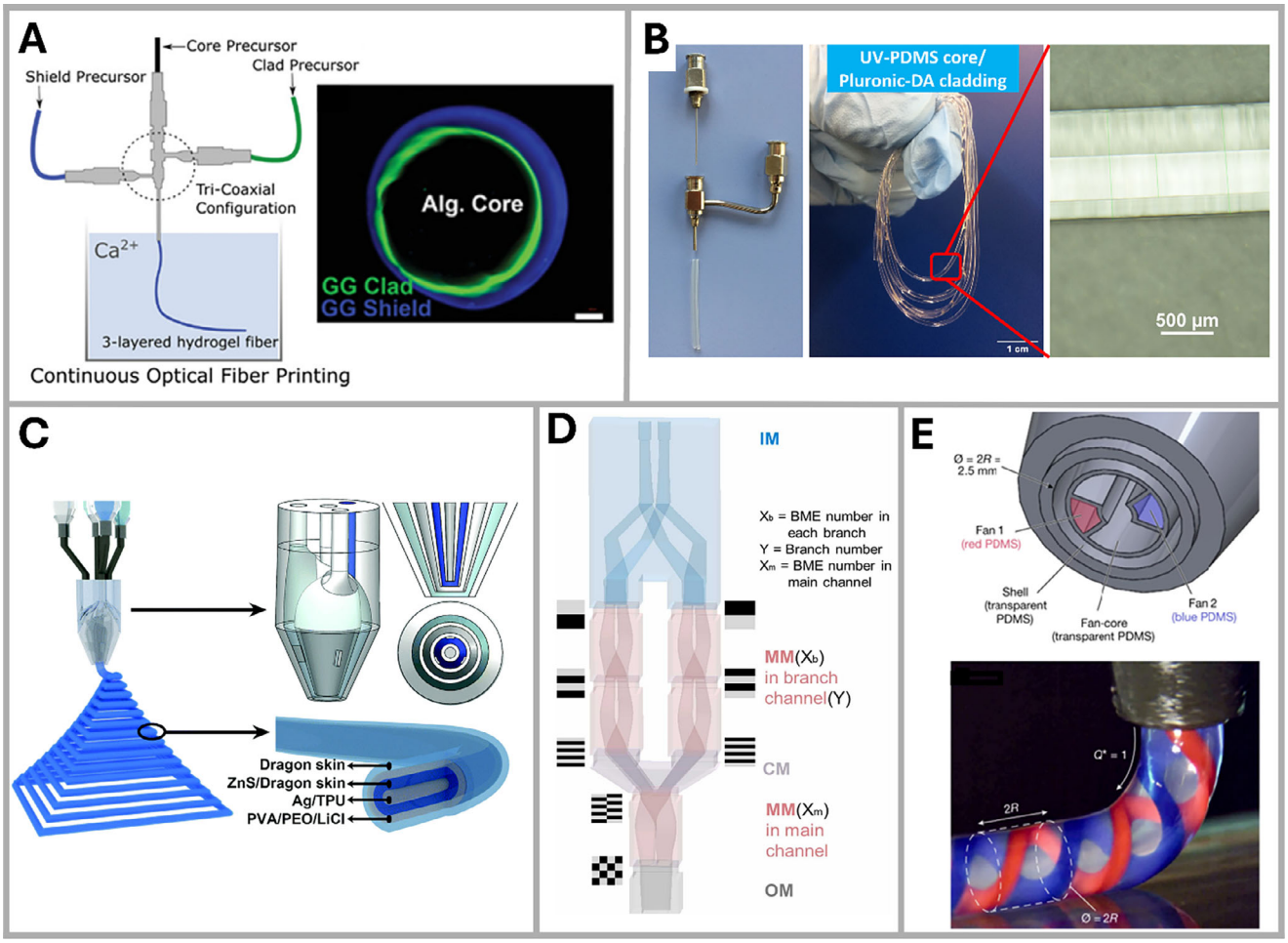

FIGURE 3 | Multimaterial coaxial extrusion printing (A) Coaxial printing of a trilayer optical fiber. Left: Desing of the nozzle; Right: Cross-section of the fiber showing the core–cladding–shield structure (Core: alginate, cladding: gellan gum, shield: gellan gum). Reproduced with permission [144]. Copyright 2021, John Wiley and Sons. (B) Coaxial nozzle used to print a PDMS/Plu-DA core-cladding fiber and images of the printed flexible waveguides. Reproduced with permission [13]. Copyright 2022, John Wiley and Sons. (C) Multicore-shell extrusion head and stretchable alternating current electroluminescent fibers. Reproduced with permission [152]. Copyright 2020, Royal Society of Chemistry. (D) Design of modular extruder head to obtain filaments with 3D architecture showing serial and parallel configuration. Reproduced with permission [153]. Copyright 2024, Elsevier. (E) Multi-material nozzle for rotational extrusion printing of PDMS filaments. Reproduced with permission [42]. Copyright 2023, Springer Nature.

layer (164 ± 10 μm), an outer conductive layer (135 μm), and an encapsulation layer (277 μm), resulting in an overall diameter of 1.5 ± 0.05 mm. The conductive layers are formulated from an ionically conductive ink based on glycerol, sodium chloride, and polyethylene glycol, while the dielectric and encapsulation layers consist of silicone elastomer. The fiber structure can be tuned by modifying nozzle dimensions, ink flow rates, and printing parameters. These fibers function as soft capacitive strain sensors with accurate, hysteresis-free responses under static and dynamic deformation, and can be readily integrated into textile systems.

The assembly of several extruder heads in series or parallel configurations allowed flexible extrusion printing of fibers into complex, multilayered architectures (Figure 3D) [156]. Two reactive silicone inks with similar rheological properties but different final mechanical properties were coextruded (soft/hard PDMS by varying ratios of epoxy/silicone). The modular printhead (Figure 3D) enabled printing scaffolds containing 4 to 128 layers, with individual layer thicknesses varying between 250 μm and 8 μm. Using this system, the researchers printed a 3D staggered woodpile structure composed of filaments made from multilayered PDMS and epoxy composites. These multilayered filaments were arranged in alternating directions to form a bidirectionally staggered lattice. Beyond enhancing mechanical toughness, the incorporation of diverse functional modules and materials opens up the potential for creating advanced programmable architectures with unique electronic, magnetic, and optothermal properties.

Rotational multimaterial 3D printing was developed to fabricate filaments containing an internal helical structure with subvoxel-level control (Figure 3E) [42]. By continuously rotating a multimaterial nozzle during the printing process, fibers with internal helicoidal structures were extruded including programmable control of helix angles and material interfaces within the filament. A dielectric elastomer ink formed the outer soft, stretchable matrix, while a conductive carbon ink was used to print the helical conductive channels inside the soft filament. Filaments were cured in situ using UV light. The core

diameters (helical structure) ranged from 250 to 700 μm and the overall filament diameter ranged from 2.5 to 5 mm. The authors printed helical dielectric elastomer actuator filaments featuring helical conductive channels embedded within a dielectric elastomer matrix. Each filament contained basic actuation units formed by soft dielectric membranes sandwiched between soft electrodes. When voltage was applied, electrostatic forces compressed the membranes, causing the actuators to contract. The same fabrication method was applied to process 3D lattice structures composed of architected filaments. In these lattices, soft acrylic ink was used to create a flexible matrix, while stiff acrylic ink formed the reinforcing spring elements. By combining stiff elements within a compliant matrix, the resulting architectures showed enhanced energy absorption and mechanical resilience.

Coaxial extrusion printing offers high adaptability for fabricating multimaterial soft optical fibers with tunable geometries and compositions, providing fine control over both optical and mechanical properties. This control is rooted in several interdependent factors: viscosity ratios and flow-rate balance dictate core–cladding concentricity [157], printing speed and nozzle alignment govern interfacial smoothness, dimensional uniformity [158], and curing kinetics—whether photopolymerization or ionic crosslinking—establish refractive-index contrast and interface sharpness [159, 160]. Together, these parameters determine propagation efficiency, numerical aperture, modal stability, and long-term transmission performance.

Despite these advantages, significant technical challenges remain. The resolution of coaxial extrusion printing is fundamentally limited by nozzle dimensions, ink rheology, and flow stability, and the presence of multiple layers in coaxial designs further restricts the minimum achievable feature size [161]. Interface distortion and uneven shell thicknesses can result in increased optical attenuation. Material compatibility adds an additional layer of complexity: stable coaxial flow requires overlapping viscosity windows and shear-thinning behavior, whereas many optically favorable elastomers and acrylates fall outside these rheological ranges [161–163]. Viscosity mismatch can induce internal flow instability and off-center core placement. Moreover, materials with slow or oxygen-sensitive curing may fail to solidify rapidly enough to maintain structural fidelity [164, 165], causing collapse or interfacial diffusion, while excessively fast-gelling inks risk premature solidification at the nozzle—an issue widely reported in coaxial hydrogel and bioprinting systems.

Extrusion printing also introduces intrinsic sources of optical loss not encountered in thermal drawing or molding [166]. Nozzle-related defects and viscoelastic recoil produce micron-scale surface roughness, increasing scattering in polymer fibers. Interfacial instabilities—including oscillations, waviness, and refractive-index gradients arising from diffusion or nonuniform curing—further degrade waveguiding performance [167, 168]. Although rapid photopolymerization improves shape retention, it may also trap interfacial defects before they relax, compounding scattering losses. Targeted improvements in nozzle engineering, pressure regulation, solvent-assisted surface reflow, and mild thermal or UV annealing could help improve the optical smoothness characteristic.

Overall, advancements in rheology-tailored precursor systems, optimized coaxial nozzle architectures, and hybrid manufacturing approaches have the potential to overcome these limitations. Such developments could ultimately yield soft multimaterial fibers with optical performance approaching that of thermally drawn polymer fibers, while preserving the structural programmability unique to extrusion-based fabrication.

4.4.2 | Segmented Extrusion of Soft Multimaterial Fibers

In segmented extrusion, fibers with compositionally different segments along the fiber length are fabricated from two or more precursor materials which are alternately fed into the nozzle—either periodically or in programmed sequences. The resulting filament contains discrete segments with different optical, mechanical, chemical, or other functional properties (Figure 2E) [46]. The concept of segmented extrusion emerged from efforts to introduce spatial heterogeneity within printed filaments, enabling localized control over composition and functionality along the fiber axis [169]. Extruding fibers with alternating compositions through a single nozzle presents new opportunities for fabricating structures with precisely tailored compositional and property gradients [161, 170]. When applied to soft optical fibers, segmented designs offer distinct optical advantages by enabling spatially programmed light transport, emission, absorption etc. along a single filament. By integrating segments with distinct optical properties—such as differences in refractive index, scattering coefficient, absorption, or fluorescence—these fibers offer light management capability in a position-dependent way that are not achievable with homogeneous waveguides [46, 92]. This segmentation allows precise control over where light is guided, attenuated, scattered, or emitted, which is particularly valuable for distributed sensing, multi-point illumination, and logic-like optical responses. For sensing applications, segments with varied mechanical or optical sensitivities can create localized strain-, pressure-, or curvature-responsive zones, enabling spatially resolved detection without complex arrays or electronics [28, 77, 92]. In biomedical contexts, patterned segments can deliver light at discrete locations for targeted phototherapy or diagnostics. Additionally, when combined with multimaterial extrusion printing, segmentation allows on-demand customization of fiber functionalities—such as alternating waveguiding and scattering regions—providing a versatile platform for designing soft photonic devices with engineered light–matter interactions along their length [46].

To enable segmented extrusion, the extrudable inks should have similar rheological properties to be extrudable at similar pressure conditions to facilitate alternating flow and prevent clogging or mixing at the interfaces. Strong adhesion between adjacent ink segments is necessary to avoid mechanical failure. In addition, the solidification mechanisms of the different inks should be compatible with each other.

Early studies adopted microfluidic printheads and multichannel nozzles to alternate between inks with distinct rheological and curing properties, establishing the foundation for multimaterial fiber printing with axial segmentation [169]. Using a microfluidic

printhead, filaments with alternating segments of viscoelastic thermocrosslinkable PDMS inks were extruded. The inks were pushed through two 200 μm channels into a microfluidic junction (200 μm expanded to 400 μm) by two opposed syringe pumps, enabling rapid switching between the inks. A key feature of the system is the design of the junction and expansion sections, which minimize the transition volume and sharpen the interfaces between the materials in the printed filaments. Filaments with diameter 400 μm and alternating features were printed. The system achieved a minimum transition length of 520 μm at flow rates of 1600 μL/min, allowing for filaments with segments of alternating composition. These pioneering demonstrations established that dynamic switching of flow inputs or modulation of pneumatic pressure allows for the formation of discrete segments within a continuous filament, enabling compositional gradients or distinct material domains without requiring post-processing assembly.

In subsequent work, the printing resolution was improved by developing a multimaterial multichannel nozzle, which enables rapid switching between multiple inks to fabricate soft materials with voxel-level control over composition and properties (Figure 4A) [44]. Up to eight inks could be extruded with a single printhead using microfluidic diode-like junctions to prevent mixing and cross-contamination. This setup processed different inks through bifurcating channel networks that converged at a junction located right before the outlet of the nozzle (≈ 200 μm). The system allowed for continuous extrusion of filaments with features of controlled length and variable composition along the filament's length (Figure 4A), with a resolution of 250 μm. Multimaterial filaments combining silicone and epoxy inks with varying mechanical properties were printed into 3D objects with spatially tailored mechanical properties. For precise deposition, the inks required a yield stress between 150 to 500 Pa and shear thinning behavior.

Using a computer-controlled pneumatic pressure controller in combination with a microfluidics-based single nozzle printhead, laminar flow-based voxelation of seven different hydrogel inks was achieved (Figure 4B) [40]. The inks consisted of gelatin methacryloyl (GelMA), alginate—with shear-thinning properties—and cellulose nanofibrils. Filaments from these inks were printed into a supporting bath of agarose or gelatin containing calcium chloride, which served as a temporary scaffold to stabilize the ink during printing. The alginate ink crosslinked upon contact with calcium chloride, while GelMA was stabilized through a UV curing step after printing. The inks merged at a junction just before being extruded through a 330 μm nozzle, which was equipped with integrated pressure valves to prevent backflow. This setup enables the fabrication of multicompartment microfibers (solid, core–shell, donut-shaped) with regions composed of two, four, or six different bioinks. These microfibers had diameters ranging from 300 to 500 μm. A long transition zone, ranging from 6 cm to 1.8 cm, was observed between printed segments of different materials at a print speed of 1400 mm/min and switching frequencies of 2.6 to 5.2 Hz.

In another study, researchers developed a dual-core coaxial nozzle to extrude fibers with a segmented core, alternating between segments of a conductive hydrogel or thermochromic elastomer, and a shell made of a thermoplastic polymer (Figure 4C) [171]. The conductive hydrogel consisted of PAM mixed with graphene oxide, while the thermochromic elastomer was silicone rubber containing thermochromic microcapsules that change color with temperature. The shell was composed of polystyrene-block-polyisoprene-block-polystyrene, which provided structural integrity by protecting the core from environmental and mechanical damage, as well as offering electrical insulation. For extrusion, a dual-core coaxial stainless-steel needle (14G) with two inner needles (22G) was used. The shell material was cured by immersion in an alcohol bath, while the core material was polymerized through thermally initiated radical polymerization by immersing the fiber in a water bath at 60°C. The fiber dimensions were adjusted by varying the flow rates during extrusion. Fibers with core/shell thicknesses of 192/796 μm and 96/1010 μm were produced, with alternating segments greater than 5 cm in length (Figure 4C). These fibers show potential for use as sensors in wearable materials and technologies.

Inspired by these methodological advances, we have recently developed segmented, side-emitting hydrogel optical fibers using multimaterial extrusion printing [46]. In our work, a Y-shaped nozzle (Figure 4D) with two inlets was designed, and a pneumatic pressure controller connected to ink-filled syringes enabled switching between the two inlet channels of the nozzle. A 23.1 w/w % solution of Plu-DA was selected as the waveguiding ink due to its shear-thinning behavior and high transparency. Plu-DA mixed with polystyrene nanoparticles (FluoSpheres) was used as the scattering ink, providing both scattering and fluorescence properties without affecting the ink's rheology. With this system, 1 mm diameter fibers were printed with segments of varying optical properties by switching between the Plu-DA waveguiding ink and the Plu-DA scattering ink (Figure 4D). The method allows the continuous fabrication of optical fibers with segment lengths as short as 500 μm in a continuous process. The segment length was controlled by adjusting the switching time between inks during printing. By varying the segment lengths and arrangement, fibers with customizable side-emission characteristics were fabricated. The printed fibers exhibited soft mechanical properties (storage modulus: 47.5 ± 2.9 kPa at 22–23°C) and effectively guided light to induce fluorescence in the surrounding 3D hydrogel environment, highlighting their potential for biomedical applications.

The spatial resolution and optical performance of segmented multimaterial fibers is highly sensitive to ink rheology, switching dynamics, nozzle design and curing mechanisms. Matching the viscosity and yield stress between inks ensures smooth switching and minimizes mixing at the interfaces, which is essential for maintaining sharp optical transitions between transparent and scattering domains. The switching frequency and flow-rate ratio determine the axial resolution of the printed segments, influencing the periodicity and uniformity of light emission or modulation [46]. Likewise, solidification kinetics—through photopolymerization, ionic crosslinking, or thermal curing—govern the refractive index profile and optical continuity across material boundaries, affecting both transmission loss and modal stability. Precise synchronization of flow control and curing thus enables reproducible formation of short, well-defined optical segments, allowing fine-tuning of side-emission intensity, attenuation length, and directionality. Continued optimization

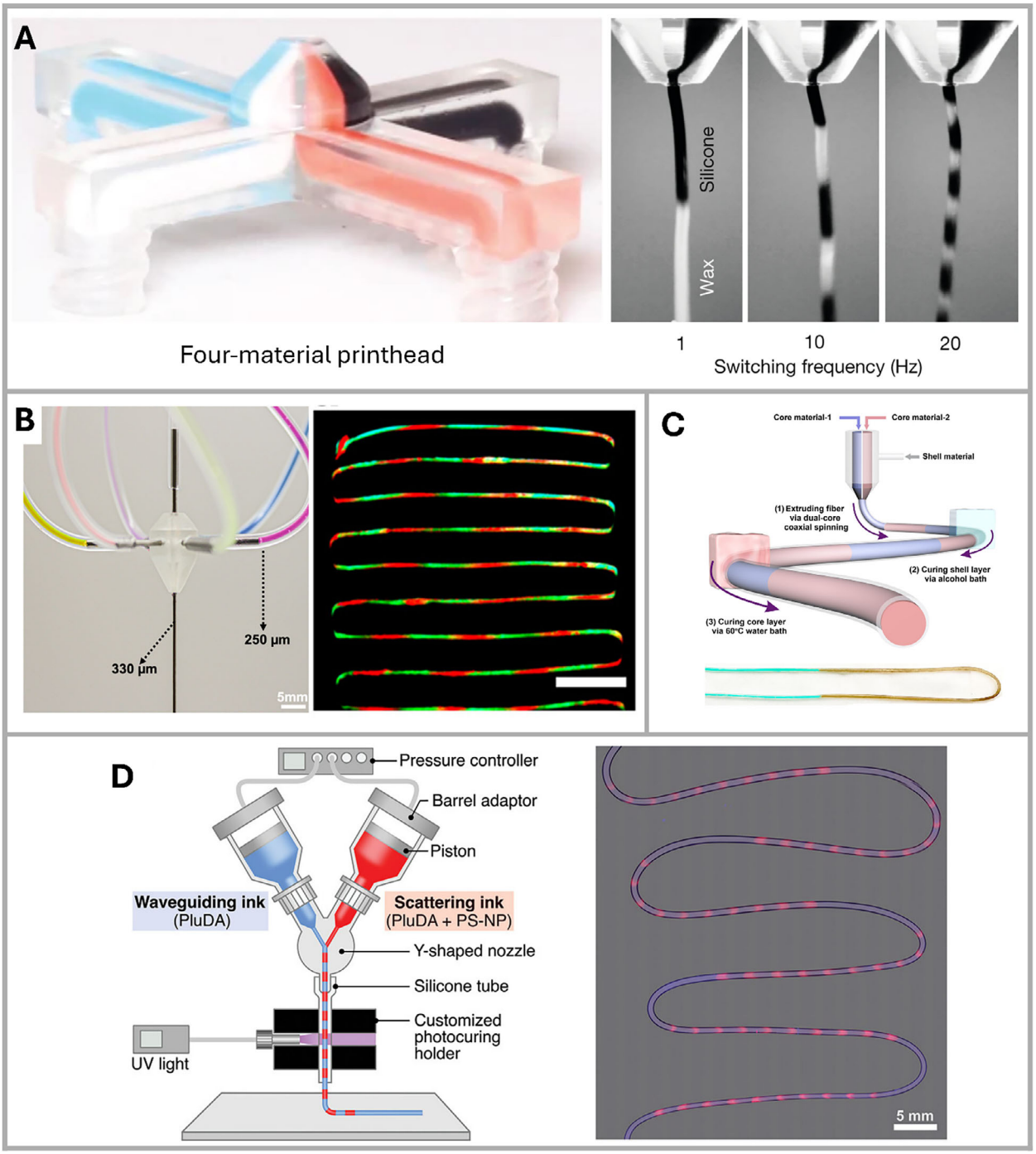

FIGURE 4 | Segmented fibers via multimaterial extrusion printing. (A) Four-material printhead and fibers. Reproduced with permission [44]. Copyright 2019, Springer Nature. (B) Single nozzle connected to seven sources for material, and printed multimaterial segmented filament. Reproduced with permission [40]. Copyright 2022, American Chemical Society. (C) Extrusion of core–shell segmented fibers through dual-core coaxial nozzle and image of the fiber containing alternating compositions of a thermochromic elastomer and a conductive hydrogel. Reproduced with permission [171]. Copyright 2020, American Chemical Society. (D) Setup for multimaterial extrusion printing and in situ photocrosslinking of the extruded fibers, and image of a side-emitting optical fiber. Reproduced with permission [46]. Copyright 2024, John Wiley and Sons.

of these coupled parameters will expand segmented extrusion printing into a robust strategy for producing programmable, multifunctional soft optical fibers capable of spatially resolved illumination, sensing, and signal modulation.

To facilitate comparison among different fabrication methods, we summarized the common parameters—including nozzle configuration, material composition, fiber geometry, and resulting functionality—in Table 1, which provides a comprehensive overview of representative multimaterial fibers fabricated by various methods. The table highlights the relationships between fiber design, fabrication strategy, material choice, geometry, and functionality, and is organized to allow readers to compare common fabrication principles

TABLE 1 | Overview of multimaterial filaments obtained by different methods.

Fiber design	Fabrication method	Material	Fiber Geometry	Function	Refs.
Coaxial fiber	Extrusion Coaxial nozzle with 4 layers	Core: PU/Ag, Cladding 1: ZnS/DS Cladding 2: PVA/PEO/LiCl Cladding 3: DS	Core: 200 μm Cladding: 200 μm for each layer Length: continuous	Stretchable electroluminescent fibers	[152]
Coaxial fiber	Extrusion rotational nozzle with helical core	Core: PDMS, urethane acrylate oligomer + carbon black Cladding: clear PDMS	Core: 0.2–0.7 mm Cladding: 2.5–5 mm Length: continuous	Actuation and filaments for lattices	[42]
Coaxial fiber	Extrusion Coaxial nozzle with 2 layers	Core: PEGDA hydrogel or PDMS Cladding: Plu-DA hydrogel	Core: 600–800 μm Cladding: 100–200 μm Length: continuous	Light guiding to activate biochemical or biological processes	[13, 53]
Coaxial fiber	Extrusion Modular printing head	Parallel-aligned layers: Soft/hard PDMS and epoxy precursor mixtures	Thickness: 8–250 μm Dimension: 1 mm × 1 mm Length: continuous	Lamellar composite filaments for printing 3D structures: like woodpile structures	[156]
Coaxial fiber	Wet-spinning with tri-coaxial nozzle	Core: alginate hydrogel with cells Cladding 1: gellan gum hydrogel Cladding 2: gellan gum hydrogel	Core: 600–800 μm Cladding: 100–200 μm Length: continuous	Real-time monitoring of cell proliferation and drug response	[144]
Coaxial fiber	Thermal drawing	Core: PMMA optical guides, metallic wires and microfluidic channels Cladding: SEBS	PMMA optical fiber: 100–200 μm Metallic wires:125 μm Microfluidic channels: 100 μm Cladding: 700–1500 μm Length: 65 cm	Soft robotic fibers for perceiving, imaging, sensing, probing electric properties, delivering fluids and tools to spatially distributed targets	[33]
Coaxial fiber	Thermal drawing	Core: PC, cyclic olefin copolymer, conductive polyethylene, Sn and hollow channel Cladding: PC	PC core: 50–200 μm Sn core: 5 μm Hollow channel: 200 μm Shell: 700 μm Length: continuous	optical stimulation, neural recording and drug delivery	[172]
Coaxial fiber	Multi-step molding	Core: silk film cladding: silk hydrogel	Core: 2 mm Cladding: 3.18 mm Length: 145 mm	/	[116]
Coaxial fiber	Molding + post coating	Core: PEGDA hydrogel Cladding: alginate hydrogel	Core: 250–1000 μm Cladding:370–1120 μm Length:	Optical sensing of blood oxygenation	[28]

(Continues)

TABLE 1 | (Continued)

Fiber design	Fabrication method	Material	Fiber Geometry	Function	Refs.
Segmented fiber	Extrusion, microfluidic printhead	Segment 1: PDMS + red pigment Segment 2: PDMS	Diameter: ≈ 420 µm Length: continuous Transition zone: 520 µm at Qp = 1600 µL/min between inks	Filaments for printing 2D and 3D structures	[169]
Segmented fiber	Extrusion, single nozzle with 4 junctions	Segment 1: mixture of silicone/epoxy/wax Segment 2: mixture of silicone/epoxy/wax	Diameter: ≈250 µm Length: continuous Transition zone: 320 µm transition length at a switching frequency of ≈ 60 Hz	Filaments for voxel printing	[44]
Segmented fiber	Extrusion, microfluidics-based single nozzle printhead	Segment 1: GelMA/Alginate/Cellulose + red pigment Segment 2: GelMA/Alginate/Cellulose + green pigment	Diameter: 300–500 µm Length: continuous Transition zone: 1.8 cm length at a switching frequency of ≈ 5.2 Hz	Tissue engineering	[40]
Segmented fiber	Extrusion, Multicore-cladding nozzle followed by 2-step curing	Segment 1: PAM with graphene oxide Segment 2: silicone rubber containing thermochromic microcapsules Cladding: polystyrene-block-polyisoprene-block-polystyrene	Segment 1: Core: 192 µm, Cladding: 796 µm Segment 2: Core: 96 µm, Shell: 1010 µm Length: continuous Transition zone: unknown	Wearable sensors for monitoring strain and body temperature	[171]
Segmented fiber	Extrusion, Y-shaped nozzle with in-situ photocuring	Segment 1: Plu-DA Segment 2: Plu-DA + polystyrene nanoparticles	Diameter: 1 mm Length: continuous Transition zone: 2.2 and 0.4 mm with switching times between 15 and 2.5 s	Side-emitting optical fibers for illumination inside tissues for photodynamic therapy	[46]

across two major classes: coaxial fibers and segmented fibers.

For coaxial fibers, the listed examples demonstrate methods such as extrusion with multi-layer coaxial nozzles, rotational or modular printheads, wet-spinning, and thermal drawing. These approaches enable precise spatial arrangement of core and cladding materials, resulting in fibers with continuous architectures and tunable diameters ranging from a few hundred micrometers to several millimeters. The materials vary from elastomeric systems (e.g., PDMS, SEBS) to thermoplastics (e.g., polymethyl methacrylate (PMMA), Polycarbonate (PC)), enabling applications in stretchable electroluminescent fibers, tissue scaffolds, light-guiding structures, and multifunctional soft robotic systems.

The segmented fibers section summarizes examples produced through extrusion-based 3D printing and microfluidic extrusion, where alternating segments with distinct compositions are printed along the fiber axis. Variations in nozzle design—such as microfluidic junctions, multicore-cladding, Y-shaped, or single-nozzle configurations—allow dynamic control over the transition length between adjacent segments (ranging from hundreds of micrometers to several millimeters). The chosen materials, including PDMS, PAM, GelMA/alginate blends, and Pluronic-based hydrogels, define the mechanical, optical, or sensing functionalities of the printed fibers. These segmented systems demonstrate the potential for applications such as tissue engineering, voxel-based printing, wearable sensors, and side-emitting optical fibers for phototherapy.

Overall, Table 1 allows readers to compare shared fabrication parameters—such as nozzle configuration, flow control, segment transition length, and continuous fiber formation—across diverse multimaterial printing strategies. It emphasizes how fabrication design directly determines fiber geometry and composition, which in turn govern mechanical compliance, optical performance, and functional versatility.

5 | Conclusions and Perspectives

Light-based technologies for in vivo diagnostics and therapy can transform modern medicine, especially through the use of soft optical fibers, which enable efficient light delivery to deep tissue sites and show high biocompatibility. Their intrinsic flexibility and mechanical compliance make them superior to rigid fibers for integration with biological environments. Soft multimaterial optical fibers further expand this potential by incorporating additional functionalities through the integration of multiple components within a single filament. The emergence of multimaterial extrusion printing technologies has opened new opportunities for creating hybrid fibers with tailored architectures and functions along and across the waveguide, with higher degrees of miniaturization and application-specific functionalities.

Despite these advances, several key challenges are to be addressed before these technologies can transition from laboratory demonstrations to widespread biomedical use. Extrusion printing inherently introduces defects such as surface roughness, interfacial waviness, and diffusion-driven refractive-index gradients, all of which affect scattering and optical loss along the wavelength. Addressing these limitations requires advances in nozzle geometry, real-time pressure control, rheology-optimized precursor inks, oxygen-tolerant photochemistry, and post-printing surface reflow or annealing strategies.

The compatibility of the optical ink with extrusion printing remains an important issue. Many optically favorable elastomers and hydrogel formulations have inappropriate viscosity ranges or curing kinetics for stable coaxial flow or rapid solidification. Precursor systems with fast-curing and oxygen-insensitivity are needed to improve print fidelity, reduce light attenuation and ensure robust interfaces.

Soft hydrogels typically have low polymer content and low refractive index. Hydrogel compositions that allow refractive-index-matching, dynamic hydrogels which allow higher polymer content while keeping compliance, or composite fiber architectures that retain interfacial stability despite a mechanical mismatch between the core and the cladding can help overcoming the tradeoff between refractive index and mechanical stability.

Structural resolution in extrusion printing depends on nozzle architecture and flow stability. Achieving coaxial fibers with diameters <200 μm or axial segments with length <500 μm is difficult due to viscosity mismatch between the core and shell inks, slow valve-switching dynamics, and diffusion-induced blurring of the interfaces. Progress in printhead engineering, valve-integrated nozzles, high-speed switching, and predictive flow modeling is crucial for better control over core–cladding concentricity, interfacial sharpness, and segment definition.

Integrating multifunctionality within a single extrusion printed filament requires reliable strategies for combining materials with disparate optical, mechanical, and electrical properties. Embedding sensing modules, scattering domains, conductive pathways, or therapeutic compartments will depend on improved intermaterial adhesion, synchronized curing schemes, and hybrid workflows that merge extrusion with molding or photopatterning.

Clinical translation introduces additional requirements beyond fabrication. Long-term biostability, compatibility with sterilization, minimally invasive implantation strategies, and the ability to manufacture fibers at scale remain largely undeveloped. Equally important is the establishment of standardized optical characterization metrics—such as optical loss, numerical aperture, and delivered irradiance in tissue—to enable meaningful comparison across different fabrication approaches and laboratories.

By addressing these material, processing, and translational challenges, extrusion-based approaches can mature into scalable and reliable platforms for next-generation flexible photonic tools. Continued innovations in materials science are likely to yield polymeric and composite inks with enhanced optical and mechanical performance, further expanding the capabilities of soft optical fibers. Ultimately, these advances will accelerate the development of minimally invasive, personalized photomedical technologies and contribute to more effective, accessible, and patient-specific clinical diagnostics and therapies.

Acknowledgements

Authors acknowledge funding from the Leibniz Association (Leibniz ScienceCampus LiveMat) and the Deutsche Forschungsgemeinschaft (SPP1425).

Open access funding enabled and organized by Projekt DEAL.

Funding

Leibniz Association (Leibniz ScienceCampus LiveMat); Deutsche Forschungsgemeinschaft (DFG, SPP1425).

Conflicts of Interest

The authors declare no conflicts of interest.

References

1. J. S. Lee, J. Kim, Y. Ye, and T. Kim, "In Vivo Fate and Intracellular Trafficking of Vaccine Delivery Systems," *Advanced Drug Delivery Reviews* 186 (2022): 114325, https://doi.org/10.1016/j.addr.2022.114325.

2. M. Lu, S. Li, Y. Liu, et al., "Advances in Phototherapy for Infectious Diseases," *Nano Today* 57 (2024): 102327, https://doi.org/10.1016/j.nantod.2024.102327.

3. G. Keiser, F. Xiong, Y. Cui, and P. P. Shum, "Review of Diverse Optical Fibers Used in Biomedical Research and Clinical Practice," *Journal of biomedical optics* 19 (2014): 080902, https://doi.org/10.1117/1.JBO.19.8.080902.

4. S. H. Yun and S. J. Kwok, "Light in Diagnosis, Therapy and Surgery," *Nature biomedical engineering* 1 (2017): 0008, https://doi.org/10.1038/s41551-016-0008.

5. S. Pearson, J. Feng, and A. Del Campo, "Lighting the Path: Light Delivery Strategies to Activate Photoresponsive Biomaterials In Vivo," *Advanced Functional Materials* 31 (2021): 2105989, https://doi.org/10.1002/adfm.202105989.

6. G. Oh, E. Chung, and S. H. Yun, "Optical Fibers for High-Resolution In Vivo Microendoscopic Fluorescence Imaging," *Optical Fiber Technology* 19 (2013): 760–771, https://doi.org/10.1016/j.yofte.2013.07.008.

7. M. R. Sarabi, N. Jiang, E. Ozturk, A. K. Yetisen, and S. Tasoglu, "Biomedical Optical Fibers," *Lab on a Chip* 21 (2021): 627–640, https://doi.org/10.1039/D0LC01155J.

8. G. Singh and A. Chanda, "Mechanical Properties of Whole-Body Soft Human Tissues: A Review," *Biomedical Materials* 16 (2021): 062004, https://doi.org/10.1088/1748-605X/ac2b7a.

9. S. Shabahang, S. Kim, and S. H. Yun, "Light-Guiding Biomaterials for Biomedical Applications," *Advanced functional materials* 28 (2018): 1706635, https://doi.org/10.1002/adfm.201706635.

10. G. Chen, K. Hou, N. Yu, et al., "Temperature-Adaptive Hydrogel Optical Waveguide With Soft Tissue-Affinity for Thermal Regulated Interventional Photomedicine," *Nature Communications* 13 (2022): 7789, https://doi.org/10.1038/s41467-022-35440-w.

11. M. Choi, J. W. Choi, S. Kim, S. Nizamoglu, S. K. Hahn, and S. H. Yun, "Light-Guiding Hydrogels for Cell-Based Sensing and Optogenetic Synthesis In Vivo," *Nature photonics* 7 (2013): 987–994, https://doi.org/10.1038/nphoton.2013.278.

12. L. Rudmann, D. Scholz, M. T. Alt, et al., "Fabrication and Characterization of PDMS Waveguides for Flexible Optrodes," *Advanced Healthcare Materials* 13 (2024): 2304513, https://doi.org/10.1002/adhm.202304513.

13. J. Feng, Y. Zheng, Q. Jiang, M. K. Włodarczyk-Biegun, S. Pearson, and A. del Campo, "Elastomeric Optical Waveguides by Extrusion Printing," *Advanced Materials Technologies* 7 (2022): 2101539, https://doi.org/10.1002/admt.202101539.

14. Y. Wang, Y. Huang, H. Bai, et al., "Biocompatible and Biodegradable Polymer Optical Fiber for Biomedical Application: A Review," *Biosensors* 11 (2021): 472, https://doi.org/10.3390/bios11120472.

15. J. Guo, C. Yang, Q. Dai, and L. Kong, "Soft and Stretchable Polymeric Optical Waveguide-Based Sensors for Wearable and Biomedical Applications," *Sensors* 19 (2019): 3771, https://doi.org/10.3390/s19173771.

16. M. S. B. Sadeque, H. K. Chowdhury, M. Rafique, et al., "Hydrogel-Integrated Optical Fiber Sensors and Their Applications: A Comprehensive Review," *Journal of Materials Chemistry C* 11 (2023): 9383–9424, https://doi.org/10.1039/D3TC01206A.

17. C. Vicentini, A.-S. Vignion-Dewalle, E. Thecua, et al., "Photodynamic Therapy for Actinic Keratosis of the Forehead and Scalp: A Randomized, Controlled, Phase II Clinical Study Evaluating the Noninferiority of a New Protocol Involving Irradiation With a Light-Emitting, Fabric-Based Device (the Flexitheralight Protocol) Compared With the Conventional Protocol Involving Irradiation With the Aktilite CL 128 Lamp," *British Journal of Dermatology* 180 (2019): 765–773, https://doi.org/10.1111/bjd.17350.

18. H. Zhao, X. Wang, Z. Geng, et al., "Dual-Function Microneedle Array for Efficient Photodynamic Therapy With Transdermal Co-Delivered Light and Photosensitizers," *Lab on a Chip* 22 (2022): 4521–4530, https://doi.org/10.1039/D2LC00505K.

19. S. J. Kwok, S. Forward, C. M. Wertheimer, et al., "Selective Equatorial Sclera Crosslinking in the Orbit Using a Metal-Coated Polymer Waveguide," *Investigative Opthalmology & Visual Science* 60 (2019): 2563–2570, https://doi.org/10.1167/iovs.19-26709.

20. J. Shen, X. Tao, D. Ying, C. Hui, and G. Wang, "Light-Emitting Fabrics Integrated With Structured Polymer Optical Fibers Treated With an Infrared CO_2 Laser," *Textile Research Journal* 83 (2013): 730–739, https://doi.org/10.1177/0040517512464299.

21. J. Shen, C. Chui, and X. Tao, "Luminous Fabric Devices for Wearable Low-Level Light Therapy," *Biomedical Optics Express* 4 (2013): 2925–2937, https://doi.org/10.1364/BOE.4.002925.

22. Y. Ran, Z. Xu, M. Chen, et al., "Fiber-Optic Theranostics (FOT): Interstitial Fiber-Optic Needles for Cancer Sensing and Therapy," *Advanced science* 9 (2022): 2200456, https://doi.org/10.1002/advs.202200456.

23. L. Wang, C. Zhong, D. Ke, et al., "Ultrasoft and Highly Stretchable Hydrogel Optical Fibers for In Vivo Optogenetic Modulations," *Advanced Optical Materials* 6 (2018): 1800427, https://doi.org/10.1002/adom.201800427.

24. M. Elsherif, A. E. Salih, M. G. Muñoz, et al., "Optical Fiber Sensors: Working Principle, Applications, and Limitations," *Advanced Photonics Research* 3 (2022): 2100371, https://doi.org/10.1002/adpr.202100371.

25. Y. J. Heo, H. Shibata, T. Okitsu, T. Kawanishi, and S. Takeuchi, "Long-Term In Vivo Glucose Monitoring Using Fluorescent Hydrogel Fibers," *Proceedings of the National Academy of Sciences* 108 (2011): 13399–13403, https://doi.org/10.1073/pnas.1104954108.

26. C. Zhang, G. G. Cano, and P. V. Braun, "Linear and Fast Hydrogel Glucose Sensor Materials Enabled by Volume Resetting Agents," *Advanced Materials* 26 (2014): 5678–5683, https://doi.org/10.1002/adma.201401710.

27. R. Boushel and C. Piantadosi, "Near-Infrared Spectroscopy for Monitoring Muscle Oxygenation," *Acta Physiologica Scandinavica* 168 (2000): 615–622, https://doi.org/10.1046/j.1365-201x.2000.00713.x.

28. M. Choi, M. Humar, S. Kim, and S. H. Yun, "Step-Index Optical Fiber Made of Biocompatible Hydrogels," *Advanced Materials* 27 (2015): 4081–4086, https://doi.org/10.1002/adma.201501603.

29. L. Wu, C. Huang, B. P. Emery, et al., "Förster Resonance Energy Transfer (FRET)-Based Small-Molecule Sensors and Imaging Agents," *Chemical Society Reviews* 49 (2020): 5110–5139, https://doi.org/10.1039/C9CS00318E.

30. A. K. Yetisen, N. Jiang, A. Fallahi, et al., "Glucose-sensitive hydrogel optical fibers functionalized with phenylboronic acid," *Advanced Materials* 29 15, (2017): 1606380.

31. J. S. Gootenberg, O. O. Abudayyeh, J. W. Lee, et al., "Nucleic Acid Detection With CRISPR-Cas13a/C2c2," *Science* 356 (2017): 438–442, https://doi.org/10.1126/science.aam9321.

32. W. Yan, A. Page, T. Nguyen-Dang, et al., "Advanced Multimaterial Electronic and Optoelectronic Fibers and Textiles," *Advanced materials* 31 (2019): 1802348, https://doi.org/10.1002/adma.201802348.

33. A. Leber, C. Dong, S. Laperrousaz, et al., "Highly Integrated Multi-Material Fibers for Soft Robotics," *Advanced Science* 10 (2023): 2204016, https://doi.org/10.1002/advs.202204016.

34. Z. Wang, M. Chen, Y. Zheng, et al., "Advanced Thermally Drawn Multimaterial Fibers: Structure-Enabled Functionalities," *Advanced Devices & Instrumentation* 2021 (2021): 9676470.

35. X. Chen, Y. Meng, S. Laperrousaz, H. Banerjee, J. Song, and F. Sorin, "Thermally Drawn Multi-Material Fibers: From Fundamental Research to Industrial Applications," *National Science Review* 11 (2024): nwae290, https://doi.org/10.1093/nsr/nwae290.

36. W. Yan, C. Dong, Y. Xiang, et al., "Thermally Drawn Advanced Functional Fibers: New Frontier of Flexible Electronics," *Materials Today* 35 (2020): 168–194, https://doi.org/10.1016/j.mattod.2019.11.006.

37. Y. Shen, Z. Wang, Z. Wang, et al., "Thermally Drawn Multifunctional Fibers: Toward the Next Generation of Information Technology," *InfoMat* 4 (2022): 12318.

38. M. B. Applegate, G. Perotto, D. L. Kaplan, and F. G. Omenetto, "Biocompatible Silk Step-Index Optical Waveguides," *Biomedical optics express* 6 (2015): 4221–4227, https://doi.org/10.1364/BOE.6.004221.

39. J. Mueller, J. R. Raney, K. Shea, and J. A. Lewis, "Architected Lattices With High Stiffness and Toughness via Multicore–Shell 3D Printing," *Advanced Materials* 30 (2018): 1705001, https://doi.org/10.1002/adma.201705001.

40. S. Hassan, E. Gomez-Reyes, E. Enciso-Martinez, et al., "Tunable and Compartmentalized Multimaterial Bioprinting for Complex Living Tissue Constructs," *ACS applied materials & interfaces* 14 (2022): 51602–51618, https://doi.org/10.1021/acsami.2c12585.

41. X. Li, J. M. Zhang, X. Yi, Z. Huang, P. Lv, and H. Duan, "Multi-material Microfluidic 3D Printing of Textured Composites With Liquid Inclusions," *Advanced Science* 6 (2019): 1800730, https://doi.org/10.1002/advs.201800730.

42. N. M. Larson, J. Mueller, A. Chortos, Z. S. Davidson, D. R. Clarke, and J. A. Lewis, "Rotational Multimaterial Printing of Filaments With Subvoxel Control," *Nature* 613 (2023): 682–688, https://doi.org/10.1038/s41586-022-05490-7.

43. T. J. Ober, D. Foresti, and J. A. Lewis, "Active Mixing of Complex Fluids at the Microscale," *Proceedings of the National Academy of Sciences* 112 (2015): 12293–12298, https://doi.org/10.1073/pnas.1509224112.

44. M. A. Skylar-Scott, J. Mueller, C. W. Visser, and J. A. Lewis, "Voxelated Soft Matter via Multimaterial Multinozzle 3D Printing," *Nature* 575 (2019): 330–335, https://doi.org/10.1038/s41586-019-1736-8.

45. I. Hassan and P. R. Selvaganapathy, "Microfluidic Printheads for Highly Switchable Multimaterial 3D Printing of Soft Materials," *Advanced Materials Technologies* 7 (2022): 2101709, https://doi.org/10.1002/admt.202101709.

46. Z. Kafrashian, S. Brück, P. Rogin, et al., "Segmented, Side-Emitting Hydrogel Optical Fibers for Multimaterial Extrusion Printing," *Advanced Materials* 37 (2025): 2309166, https://doi.org/10.1002/adma.202309166.

47. Y. Koike, *Fundamentals of Plastic Optical Fibers* (John Wiley & Sons, 2014), https://doi.org/10.1002/9783527646500.

48. N. Tanio and Y. Koike, "What Is the Most Transparent Polymer?," *Polymer Journal* 32 (2000): 43–50, https://doi.org/10.1295/polymj.32.43.

49. H. Ma, A. Y. Jen, and L. R. Dalton, "Polymer-Based Optical Waveguides: Materials, Processing, and Devices," *Advanced materials* 14 (2002): 1339–1365, https://doi.org/10.1002/1521-4095(20021002)14:19%3c1339::AID-ADMA1339%3e3.0.CO;2-O.

50. G. P. Agrawal, *Fiber-Optic Communication Systems* (John Wiley & Sons, 2012).

51. J. Zubia and J. Arrue, "Plastic Optical Fibers: An Introduction to Their Technological Processes and Applications," *Optical fiber technology* 7 (2001): 101–140, https://doi.org/10.1006/ofte.2000.0355.

52. G. Hougham, G. Tesoro, A. Viehbeck, and J. Chapple-Sokol, "Polarization Effects of Fluorine on the Relative Permittivity in Polyimides," *Macromolecules* 27 (1994): 5964–5971, https://doi.org/10.1021/ma00099a006.

53. J. Feng, Y. Zheng, S. Bhusari, M. Villiou, S. Pearson, and A. del Campo, "Printed Degradable Optical Waveguides for Guiding Light Into Tissue," *Advanced functional materials* 30 (2020): 2004327, https://doi.org/10.1002/adfm.202004327.

54. P. Y. M. Yew, P. L. Chee, Q. Lin, et al., "Hydrogel for Light Delivery in Biomedical Applications," *Bioactive Materials* 37 (2024): 407–423, https://doi.org/10.1016/j.bioactmat.2024.03.031.

55. R. Khan, B. Gul, S. Khan, H. Nisar, and I. Ahmad, "Refractive Index of Biological Tissues: Review, Measurement Techniques, and Applications," *Photodiagnosis and photodynamic therapy* 33 (2021): 102192, https://doi.org/10.1016/j.pdpdt.2021.102192.

56. S. Cheng, E. C. Clarke, and L. E. Bilston, "Rheological Properties of the Tissues of the Central Nervous System: A Review," *Medical engineering & physics* 30 (2008): 1318, https://doi.org/10.1016/j.medengphy.2008.06.003.

57. S. Fleming, M. Large, and A. Stefani, "Polyurethane optical fiber sensors. Optical Sensors, 2019; Optica Publishing Group: p STh5A. 1", https://doi.org/10.1364/SENSORS.2019.STh5A.1.

58. H. Chang, L. Meng, C. Shao, C. Cui, and J. Yang, "Physically Cross-Linked Silk Hydrogels With High Solid Content and Excellent Mechanical Properties via a Reverse Dialysis Concentrated Procedure," *ACS Sustainable Chemistry & Engineering* 7 (2019): 13324–13332, https://doi.org/10.1021/acssuschemeng.9b02576.

59. D. Su, M. Yao, J. Liu, Y. Zhong, X. Chen, and Z. Shao, "Enhancing Mechanical Properties of Silk Fibroin Hydrogel Through Restricting the Growth of β-Sheet Domains," *ACS applied materials & interfaces* 9 (2017): 17489–17498, https://doi.org/10.1021/acsami.7b04623.

60. Z. Zhu, S. Ling, J. Yeo, et al., "High-Strength, Durable All-Silk Fibroin Hydrogels With Versatile Processability Toward Multifunctional Applications," *Advanced functional materials* 28 (2018): 1704757, https://doi.org/10.1002/adfm.201704757.

61. K. Luo, Y. Yang, and Z. Shao, "Physically Crosslinked Biocompatible Silk-Fibroin-Based Hydrogels With High Mechanical Performance," *Advanced Functional Materials* 26 (2016): 872–880, https://doi.org/10.1002/adfm.201503450.

62. I. Karakutuk, F. Ak, and O. Okay, "Diepoxide-Triggered Conformational Transition of Silk Fibroin: Formation of Hydrogels," *Biomacromolecules* 13 (2012): 1122–1128, https://doi.org/10.1021/bm300006r.

63. M. Reimer and C. Zollfrank, "Cellulose for Light Manipulation: Methods, Applications, and Prospects," *Advanced Energy Materials* 11 (2021): 2003866, https://doi.org/10.1002/aenm.202003866.

64. H. Orelma, A. Hokkanen, I. Leppänen, K. Kammiovirta, M. Kapulainen, and A. Harlin, "Optical Cellulose Fiber Made From Regenerated Cellulose and Cellulose Acetate for Water Sensor Applications," *Cellulose* 27 (2020): 1543–1553, https://doi.org/10.1007/s10570-019-02882-3.

65. A. Jain, A. H. Yang, and D. Erickson, "Gel-Based Optical Waveguides With Live Cell Encapsulation and Integrated Microfluidics," *Optics letters* 37 (2012): 1472–1474, https://doi.org/10.1364/OL.37.001472.

66. A. K. Manocchi, P. Domachuk, F. G. Omenetto, and H. Yi, "Facile Fabrication of Gelatin-Based Biopolymeric Optical Waveguides," *Biotechnology and bioengineering* 103 (2009): 725–732, https://doi.org/10.1002/bit.22306.

67. E. Fujiwara, T. D. Cabral, M. Sato, H. Oku, and C. M. Cordeiro, "Agarose-Based Structured Optical Fibre," *Scientific reports* 10 (2020): 7035, https://doi.org/10.1038/s41598-020-64103-3.

68. J.-Y. Sun, X. Zhao, W. R. Illeperuma, et al., "Highly Stretchable and Tough Hydrogels," *Nature* 489 (2012): 133–136, https://doi.org/10.1038/nature11409.

69. R. T. Chen, W. Phillips, T. Jannson, and D. Pelka, "Integration of Holographic Optical Elements With Polymer Gelatin Waveguides on Gaas, Linbo_3, Glass, and Aluminum," *Optics letters* 14 (1989): 892–894, https://doi.org/10.1364/OL.14.000892.

70. K. Yue, G. Trujillo-de Santiago, M. M. Alvarez, A. Tamayol, N. Annabi, and A. Khademhosseini, "Synthesis, Properties, and Biomedical Applications of Gelatin Methacryloyl (Gelma) Hydrogels," *Biomaterials* 73 (2015): 254–271, https://doi.org/10.1016/j.biomaterials.2015.08.045.

71. P. Liu, H. Shen, Y. Zhi, et al., "3D Bioprinting and in Vitro Study of Bilayered Membranous Construct with Human Cells-Laden Alginate/Gelatin Composite hydrogels," *Colloids and Surfaces B: Biointerfaces* 181 (2019): 1026–1034, https://doi.org/10.1016/j.colsurfb.2019.06.069.

72. S. Pawde and K. Deshmukh, "Characterization of Polyvinyl Alcohol/Gelatin Blend Hydrogel Films for Biomedical Applications," *Journal of Applied Polymer Science* 109 (2008): 3431–3437, https://doi.org/10.1002/app.28454.

73. L.-H. Fu, C. Qi, M.-G. Ma, and P. Wan, "Multifunctional Cellulose-Based Hydrogels for Biomedical Applications," *Journal of Materials Chemistry B* 7 (2019): 1541–1562, https://doi.org/10.1039/C8TB02331J.

74. L. Zhou, H. Ramezani, M. Sun, et al., "3d Printing of High-Strength Chitosan Hydrogel Scaffolds Without any Organic Solvents," *Biomaterials Science* 8 (2020): 5020–5028, https://doi.org/10.1039/D0BM00896F.

75. R. Gupta and N. J. Goddard, "A Study of Diffraction-Based Chitosan Leaky Waveguide (LW) Biosensors," *The Analyst* 146 (2021): 4964–4971, https://doi.org/10.1039/D1AN00940K.

76. T. Shu, K. Zheng, Z. Zhang, et al., "Birefringent Silk Fibroin Hydrogel Constructed via Binary Solvent-Exchange-Induced Self-Assembly," *Biomacromolecules* 22 (2021): 1955–1965, https://doi.org/10.1021/acs.biomac.1c00065.

77. J. Guo, B. Zhou, C. Yang, Q. Dai, and L. Kong, "Stretchable and Temperature-Sensitive Polymer Optical Fibers for Wearable Health Monitoring," *Advanced Functional Materials* 29 (2019): 1902898, https://doi.org/10.1002/adfm.201902898.

78. D. Shan, C. Zhang, S. Kalaba, et al., "Flexible Biodegradable Citrate-Based Polymeric Step-Index Optical Fiber," *Biomaterials* 143 (2017): 142–148, https://doi.org/10.1016/j.biomaterials.2017.08.003.

79. F. Abbasi, H. Mirzadeh, and A.-A. Katbab, "Modification of Polysiloxane Polymers for Biomedical Applications: A Review," *Polymer International* 50 (2001): 1279–1287, https://doi.org/10.1002/pi.783.

80. J. Missinne, S. Kalathimekkad, B. Van Hoe, E. Bosman, J. Vanfleteren, and G. Van Steenberge, "Stretchable Optical Waveguides," *Optics Express* 22 (2014): 4168–4179, https://doi.org/10.1364/OE.22.004168.

81. L. Y. Tyng, M. R. Ramli, M. B. H. Othman, R. Ramli, Z. A. M. Ishak, and Z. Ahmad, "Effect of Crosslink Density on the Refractive Index of a Polysiloxane Network Based on 2,4,6,8-tetramethyl-2,4,6,8-tetravinylcyclotetrasiloxane," *Polymer International* 62 (2013): 382.

82. C. A. Zimmermann, K. N. Amouzou, and B. Ung, "Recent Advances in PDMS Optical Waveguides: Properties, Fabrication, and Applications," *Advanced Optical Materials* 13 (2025): 2401975, https://doi.org/10.1002/adom.202401975.

83. X. Li and J. P. Gong, "Design Principles for Strong and Tough Hydrogels," *Nature Reviews Materials* 9 (2024): 380–398, https://doi.org/10.1038/s41578-024-00672-3.

84. M. L. Torres-Mapa, M. Singh, O. Simon, et al., "Fabrication of a Monolithic Lab-on-a-Chip Platform With Integrated Hydrogel Waveguides for Chemical Sensing," *Sensors* 19 (2019): 4333, https://doi.org/10.3390/s19194333.

85. X. Shi, L. Ma, Y. Li, et al., "Double Hydrogen-Bonding Reinforced High-Performance Supramolecular Hydrogel Thermocell for Self-Powered Sensing Remote-Controlled by Light," *Advanced Functional Materials* 33 (2023): 2211720, https://doi.org/10.1002/adfm.202211720.

86. Q. Zhang, Y. Wang, A. Mateescu, et al., "Biosensor Based on Hydrogel Optical Waveguide Spectroscopy for the Detection of 17β-Estradiol," *Talanta* 104 (2013): 149–154, https://doi.org/10.1016/j.talanta.2012.11.017.

87. W. Mao, X. Cai, R. Pan, et al., "Light-Enhanced Transparent Hydrogel for Uric Acid and Glucose Detection by Four Different Analytical Platforms," *Analytica Chimica Acta* 1239 (2023): 340717, https://doi.org/10.1016/j.aca.2022.340717.

88. Y. Zhang, Z. Xu, Y. Yuan, et al., "Flexible Antiswelling Photothermal-Therapy Mxene Hydrogel-Based Epidermal Sensor for Intelligent Human–Machine Interfacing," *Advanced Functional Materials* 33 (2023): 2300299, https://doi.org/10.1002/adfm.202300299.

89. A. Francone, T. Kehoe, I. Obieta, et al., "Integrated 3D Hydrogel Waveguide Out-Coupler by Step-and-Repeat Thermal Nanoimprint Lithography: A Promising Sensor Device for Water and pH," *Sensors* 18 (2018): 3240, https://doi.org/10.3390/s18103240.

90. J. Guo, M. Zhou, and C. Yang, "Fluorescent Hydrogel Waveguide for On-Site Detection of Heavy Metal Ions," *Scientific reports* 7 (2017): 7902, https://doi.org/10.1038/s41598-017-08353-8.

91. J. Guo, H. Huang, M. Zhou, C. Yang, and L. Kong, "Quantum Dots-Doped Tapered Hydrogel Waveguide for Ratiometric Sensing of Metal Ions," *Analytical chemistry* 90 (2018): 12292–12298, https://doi.org/10.1021/acs.analchem.8b03787.

92. J. Guo, X. Liu, N. Jiang, et al., "Highly Stretchable, Strain Sensing Hydrogel Optical Fibers," *Advanced Materials* 28 (2016): 10244–10249, https://doi.org/10.1002/adma.201603160.

93. N. Jiang, R. Ahmed, A. A. Rifat, et al., "Functionalized Flexible Soft Polymer Optical Fibers for Laser Photomedicine," *Advanced Optical Materials* 6 (2018): 1701118, https://doi.org/10.1002/adom.201701118.

94. S. Johannsmeier, M. Torres, T. Ripken, D. Heinemann, and A. Heisterkamp, "Hydrogels for Efficient Light Delivery in Optogenetic Applications," in *Optogenetics and Optical Manipulation*, (SPIE, 2018).

95. M. Zhou, J. Guo, and C. Yang, "Ratiometric Fluorescence Sensor for Fe3+ Ions Detection Based on Quantum Dot-Doped Hydrogel Optical Fiber," *Sensors and Actuators B: Chemical* 264 (2018): 52–58, https://doi.org/10.1016/j.snb.2018.02.119.

96. L. Zhao, J. Gan, T. Xia, et al., "A Luminescent Metal–Organic Framework Integrated Hydrogel Optical Fibre as a Photoluminescence Sensing Platform for Fluorescence Detection," *Journal of Materials Chemistry C* 7 (2019): 897–904, https://doi.org/10.1039/C8TC05154B.

97. M. Elsherif, M. U. Hassan, A. K. Yetisen, and H. Butt, "Hydrogel Optical Fibers for Continuous Glucose Monitoring," *Biosensors and Bioelectronics* 137 (2019): 25–32, https://doi.org/10.1016/j.bios.2019.05.002.

98. M. Elsherif, R. Moreddu, M. U. Hassan, A. K. Yetisen, and H. Butt, "Real-Time Optical Fiber Sensors Based on Light Diffusing Microlens Arrays," *Lab on a Chip* 19 (2019): 2060–2070, https://doi.org/10.1039/C9LC00242A.

99. J. Jung, M. Park, D. Kim, and Y.-L. Park, "Optically Sensorized Elastomer Air Chamber for Proprioceptive Sensing of Soft Pneumatic Actuators," *IEEE Robotics and Automation Letters* 5 (2020): 2333–2340, https://doi.org/10.1109/LRA.2020.2970984.

100. J. Guo, C. Shang, S. Gao, Y. Zhang, B. Fu, and L. Xu, "Flexible Plasmonic Optical Tactile Sensor for Health Monitoring and Artificial Haptic Perception," *Advanced Materials Technologies* 8 (2023): 2201506, https://doi.org/10.1002/admt.202201506.

101. M. Ramuz, B. C. Tee, J. B. Tok, and Z. Bao, "Transparent, Optical, Pressure-Sensitive Artificial Skin for Large-Area Stretchable Electronics," *Advanced Materials* 24 (2012): 3223–3227, https://doi.org/10.1002/adma.201200523.

102. C. To, T. L. Hellebrekers, and Y.-L. Park, "Highly stretchable optical sensors for pressure, strain, and curvature measurement, 2015 IEEE/RSJ international conference on intelligent robots and systems (IROS). IEEE", 2015: 5898–5903, https://doi.org/10.1109/IROS.2015.7354215.

103. S. J. Kwok, M. Kim, H. H. Lin, et al., "Flexible Optical Waveguides for Uniform Periscleral Cross-Linking," *Investigative Opthalmology & Visual Science* 58 (2017): 2596–2602, https://doi.org/10.1167/iovs.17-21559.

104. J. Guo, M. Niu, and C. Yang, "Highly Flexible and Stretchable Optical Strain Sensing for Human Motion Detection," *Optica* 4 (2017): 1285–1288, https://doi.org/10.1364/OPTICA.4.001285.

105. M. Kolle, A. Lethbridge, M. Kreysing, J. J. Baumberg, J. Aizenberg, and P. Vukusic, "Bio-Inspired Band-Gap Tunable Elastic Optical Multilayer Fibers," *Advanced Materials* 25 (2013): 2239–2245, https://doi.org/10.1002/adma.201203529.

106. J. Missinne, G. Van Steenberge, B. Van Hoe, et al., "An array waveguide sensor for artificial optical skins. Photonics Packaging, Integration, and Interconnects IX, 2009; SPIE", Vol. 7221, pp. 22–30, https://doi.org/10.1117/12.809154.

107. H. Zhao, K. O'brien, S. Li, and R. F. Shepherd, "Optoelectronically Innervated Soft Prosthetic Hand via Stretchable Optical Waveguides," *Science robotics* 1 (2016): aai7529.

108. A. Leber, B. Cholst, J. Sandt, N. Vogel, and M. Kolle, "Stretchable Thermoplastic Elastomer Optical Fibers for Sensing of Extreme Deformations," *Advanced Functional Materials* 29 (2019): 1802629, https://doi.org/10.1002/adfm.201802629.

109. S. Nizamoglu, M. C. Gather, M. Humar, et al., "Bioabsorbable Polymer Optical Waveguides for Deep-Tissue Photomedicine," *Nature communications* 7 (2016): 10374, https://doi.org/10.1038/ncomms10374.

110. M. Kim, J. An, K. S. Kim, et al., "Optical Lens-Microneedle Array for Percutaneous Light Delivery," *Biomedical optics express* 7 (2016): 4220–4227, https://doi.org/10.1364/BOE.7.004220.

111. A. Gierej, M. Vagenende, A. Filipkowski, et al., "Poly(D,L-Lactic Acid) (PDLLA) Biodegradable and Biocompatible Polymer Optical Fiber," *Journal of Lightwave Technology* 37 (2019): 1916–1923, https://doi.org/10.1109/JLT.2019.2895220.

112. R. Fu, W. Luo, R. Nazempour, et al., "Implantable and Biodegradable Poly(l -lactic acid) Fibers for Optical Neural Interfaces," *Advanced Optical Materials* 6 (2018): 1700941, https://doi.org/10.1002/adom.201700941.

113. W. J. Choi, K. S. Park, and B. H. Lee, "Light-Guided Localization Within Tissue Using Biocompatible Surgical Suture Fiber as an Optical Waveguide," *Journal of Biomedical Optics* 19 (2014): 090503, https://doi.org/10.1117/1.JBO.19.9.090503.

114. S. Shabahang, S. Forward, and S.-H. Yun, "Polyethersulfone Optical Fibers With Thermally Induced Microbubbles for Custom Side-Scattering Profiles," *Optics express* 27 (2019): 7560–7567, https://doi.org/10.1364/OE.27.007560.

115. J. Feng, Q. Jiang, P. Rogin, P. W. de Oliveira, and A. Del Campo, "Printed Soft Optical Waveguides of PLA Copolymers for Guiding Light Into Tissue," *ACS applied materials & interfaces* 12 (2020): 20287–20294, https://doi.org/10.1021/acsami.0c03903.

116. S. T. Parker, P. Domachuk, J. Amsden, et al., "Biocompatible silk printed optical waveguides," *Advanced Materials* 2123 (2009), https://doi.org/10.1002/adma.200801580.

117. X. Qiao, Z. Qian, J. Li, et al., "Synthetic Engineering of Spider Silk Fiber as Implantable Optical Waveguides for Low-Loss Light Guiding," *ACS applied materials & interfaces* 9 (2017): 14665–14676, https://doi.org/10.1021/acsami.7b01752.

118. V. Prajzler, K. Min, S. Kim, and P. Nekvindova, "The Investigation of the Waveguiding Properties of Silk Fibroin From the Visible to Near-Infrared Spectrum," *Materials* 11 (2018): 112, https://doi.org/10.3390/ma11010112.

119. X. Li, J. Qin, and Y. Hu, "Switch-On Hydrogel Biosensor Based on Self-Assembly Mn-Doped ZnS QDs and Cellulose Nanofibrils for Glutathione Detection," *Microchemical Journal* 191 (2023): 108763, https://doi.org/10.1016/j.microc.2023.108763.

120. S. Kujala, A. Mannila, L. Karvonen, K. Kieu, and Z. Sun, "Natural Silk as a Photonics Component: A Study on Its Light Guiding and Nonlinear Optical Properties," *Scientific reports* 6 (2016): 22358, https://doi.org/10.1038/srep22358.

121. N. Huby, V. Vié, A. Renault, et al., "Native Spider Silk as a Biological Optical Fiber," *Applied Physics Letters* 102 (2013): 123702.

122. K. H. Tow, D. M. Chow, F. Vollrath, I. Dicaire, T. Gheysens, and L. Thévenaz, "Towards a New Generation of Fibre-Optic Chemical Sensors Based on Spider Silk Threads," *2017 25th Optical Fiber Sensors Conference (OFS)*, (IEEE, 2017).

123. K. H. Tow, D. M. Chow, F. Vollrath, I. Dicaire, T. Gheysens, and L. Thévenaz, "Exploring the Use of Native Spider Silk as an Optical Fiber for Chemical Sensing," *Journal of Lightwave Technology* 36 (2017): 1138–1144, https://doi.org/10.1109/JLT.2017.2756095.

124. A. Mironenko, E. Modin, A. Sergeev, S. Voznesenskiy, and S. Bratskaya, "Fabrication and Optical Properties of Chitosan/Ag Nanoparticles Thin Film Composites," *Chemical Engineering Journal* 244 (2014): 457–463, https://doi.org/10.1016/j.cej.2014.01.094.

125. A. Y. Mironenko, A. Sergeev, A. Nazirov, E. Modin, S. Voznesenskiy, and S. Y. Bratskaya, "H2S Optical Waveguide Gas Sensors Based on Chitosan/Au and Chitosan/Ag Nanocomposites," *Sensors and Actuators B: Chemical* 225 (2016): 348–353, https://doi.org/10.1016/j.snb.2015.11.073.

126. A. Dupuis, N. Guo, Y. Gao, et al., "Prospective for Biodegradable Microstructured Optical Fibers," *Optics letters* 32 (2006): 109–111, https://doi.org/10.1364/OL.32.000109.

127. M. Reimer, D. Van Opdenbosch, and C. Zollfrank, "Fabrication of Cellulose-Based Biopolymer Optical Fibers and Their Theoretical Attenuation Limit," *Biomacromolecules* 22 (2021): 3297–3312, https://doi.org/10.1021/acs.biomac.1c00398.

128. A. K. Jaiswal, A. Hokkanen, M. Kapulainen, A. Khakalo, O. I. Nonappa, and H. Orelma, "Carboxymethyl Cellulose (CMC) Optical Fibers for Environment Sensing and Short-Range Optical Signal Transmission," *ACS applied materials & interfaces* 14 (2022): 3315–3323, https://doi.org/10.1021/acsami.1c22227.

129. V. Hynninen, S. Chandra, S. Das, et al., "Luminescent Gold Nanocluster-Methylcellulose Composite Optical Fibers with Low Attenuation Coefficient and High Photostability," *Small* 17 (2021): 2005205.

130. J. Patrakka, V. Hynninen, M. Lahtinen, A. Hokkanen, H. Orelma, and Z. Sun, "Mechanically Robust Biopolymer Optical Fibers With Enhanced Performance in the Near-Infrared Region," *ACS Applied Materials & Interfaces* 16 (2024): 42704–42716, https://doi.org/10.1021/acsami.4c08879.

131. J. Patrakka, V. Hynninen, and P. Huttunen, "Biopolymer Optical Fibers for High-Sensitivity Quantitative Humidity Monitoring," *ACS Applied Materials & Interfaces* 17 (2025): 49816–49828, https://doi.org/10.1021/acsami.5c10056.

132. X. Wang, Z. Li, and L. Su, "Soft Optical Waveguides for Biomedical Applications, Wearable Devices, and Soft Robotics: A Review," *Advanced Intelligent Systems* 6 (2024): 2300482, https://doi.org/10.1002/aisy.202300482.

133. C. Faccini de Lima, L. A. van der Elst, V. N. Koraganji, M. Zheng, M. G. Kurtoglu, and A. Gumennik, "Towards Digital Manufacturing of Smart Multimaterial Fibers," *Nanoscale Research Letters* 14 (2019): 209, https://doi.org/10.1186/s11671-019-3031-x.

134. Y. Chu, L. Dong, Y. Luo, J. Zhang, and G.-D. Peng, *Hybrid Planar-3D Waveguiding Technologies* (IntechOpen, 2022).

135. I. Martincek, D. Pudis, and M. Chalupova, "Technology for the Preparation of PDMS Optical Fibers and Some Fiber Structures," *IEEE Photonics technology letters* 26 (2014): 1446–1449, https://doi.org/10.1109/LPT.2014.2326695.

136. S. Shabahang, F. Clouser, F. Shabahang, and S. H. Yun, "Single-Mode, 700%-Stretchable, Elastic Optical Fibers Made of Thermoplastic

Elastomers," *Advanced Optical Materials* 9 (2021): 2100270, https://doi.org/10.1002/adom.202100270.

137. C. Strutynski, M. Evrard, F. Désévédavy, et al., "4D Optical Fibers Based on Shape-Memory Polymers," *Nature Communications* 14 (2023): 6561, https://doi.org/10.1038/s41467-023-42355-7.

138. H. Bai, S. Li, J. Barreiros, Y. Tu, C. R. Pollock, and R. F. Shepherd, "Stretchable Distributed Fiber-Optic Sensors," *Science* 370 (2020): 848–852, https://doi.org/10.1126/science.aba5504.

139. M. Reimer, K. Mayer, D. Van Opdenbosch, T. Scheibel, and C. Zollfrank, "Biocompatible Optical Fibers Made of Regenerated Cellulose and Recombinant Cellulose-Binding Spider Silk," *Biomimetics* 8 (2023): 37, https://doi.org/10.3390/biomimetics8010037.

140. K. Duan, Y. Guan, Q. Wang, et al., "Reducing Fiber Scattering Loss Through Hot-Diffusion: A Study on Eliminating Core–Cladding Interface Defects," *Optics Letters* 50 (2025): 2582–2585, https://doi.org/10.1364/OL.559151.

141. M. Beckers, T. Schlüter, T. Vad, T. Gries, and C.-A. Bunge, "An Overview on Fabrication Methods for Polymer Optical Fibers," *Polymer International* 64 (2015): 25–36, https://doi.org/10.1002/pi.4805.

142. M. F. Alexandre-Franco, R. Kouider, R. K. Al-Karany, E. M. Cuerda-Correa, and A. Al-Kassir, "Recent Advances in Polymer Science and Fabrication Processes for Enhanced Microfluidic Applications: An Overview," *Micromachines* 15 (2024): 1137, https://doi.org/10.3390/mi15091137.

143. P. Akrami, A. I. Adamu, G. Woyessa, H. K. Rasmussen, O. Bang, and C. Markos, "All-Polymer Multimaterial Optical Fiber Fabrication for High Temperature Applications," *Optical Materials Express* 11 (2021): 345–354, https://doi.org/10.1364/OME.414973.

144. C. F. Guimarães, R. Ahmed, A. Mataji-Kojouri, et al., "Engineering Polysaccharide-Based Hydrogel Photonic Constructs: From Multiscale Detection to the Biofabrication of Living Optical Fibers," *Advanced Materials* 33 (2021): 2105361, https://doi.org/10.1002/adma.202105361.

145. Y. Zhang, H. Lu, M. Zhang, et al., "In Situ Mineralizing Spinning of Strong and Tough Silk Fibers for Optical Waveguides," *ACS Nano* 17 (2023): 5905–5912, https://doi.org/10.1021/acsnano.2c12855.

146. L. Lu, S. Fan, L. Geng, X. Yao, and Y. Zhang, "Low-Loss Light-Guiding, Strong Silk Generated by a Bioinspired Microfluidic Chip," *Chemical Engineering Journal* 405 (2021): 126793, https://doi.org/10.1016/j.cej.2020.126793.

147. A. R. Shirvan, A. Nouri, and A. Sutti, "A Perspective on the Wet Spinning Process and its Advancements in Biomedical Sciences," *European Polymer Journal* 181 (2022): 111681, https://doi.org/10.1016/j.eurpolymj.2022.111681.

148. D. Puppi and F. Chiellini, "Wet-Spinning of Biomedical Polymers: From Single-Fibre Production to Additive Manufacturing of Three-Dimensional Scaffolds," *Polymer International* 66 (2017): 1690–1696, https://doi.org/10.1002/pi.5332.

149. K. Sharma, W. Wang, S. Valet, et al., "Microfluidic Wet Spinning of Soft Polydimethylsiloxane Polymer Optical Fibers," *Materials & Design* 248 (2024): 113466, https://doi.org/10.1016/j.matdes.2024.113466.

150. C. S. Miranda, A. F. G. Silva, S. M. Pereira-Lima, S. P. Costa, N. C. Homem, and H. P. Felgueiras, "Tunable Spun Fiber Constructs in Biomedicine: Influence of Processing Parameters in the Fibers' Architecture," *Pharmaceutics* 14 (2022): 164, https://doi.org/10.3390/pharmaceutics14010164.

151. W. Ding, J. Sun, G. Chen, et al., "Stretchable Multi-Luminescent Fibers With AIEgens," *Journal of Materials Chemistry C* 7 (2019): 10769–10776, https://doi.org/10.1039/C9TC03461G.

152. D. Liu, J. Ren, J. Wang, et al., "Customizable and Stretchable Fibre-Shaped Electroluminescent Devices via Mulitcore-Shell Direct ink Writing," *Journal of Materials Chemistry C* 8 (2020): 15092–15098, https://doi.org/10.1039/D0TC03078C.

153. J. Ren, D. Liu, B. Zhang, et al., "Multimaterial Extrusion of Programmable Periodic Filament Structures via Modularly Designed Extruder Heads," *Additive Manufacturing* 87 (2024): 104234, https://doi.org/10.1016/j.addma.2024.104234.

154. D. J. Lorang, D. Tanaka, C. M. Spadaccini, K. A. Rose, N. J. Cherepy, and J. A. Lewis, "Photocurable Liquid Core–Fugitive Shell Printing of Optical Waveguides," *Advanced Materials* 23 (2011): 5055–5058, https://doi.org/10.1002/adma.201102411.

155. A. Frutiger, J. T. Muth, D. M. Vogt, et al., "Capacitive Soft Strain Sensors via Multicore–Shell Fiber Printing," *Advanced Materials* 27 (2015): 2440–2446, https://doi.org/10.1002/adma.201500072.

156. J. Ren, D. Liub, B. Zhangb, et al., "Multimaterial Extrusion of Programmable Periodic Filament Structures via Modularly Designed Extruder Heads," *Additive Manufacturing* 87 (2024): 104234, https://doi.org/10.1016/j.addma.2024.104234.

157. A. C. Taylor, S. Beirne, G. Alici, and G. G. Wallace, "System and Process Development for Coaxial Extrusion in Fused Deposition Modelling," *Rapid Prototyping Journal* 23 (2017): 543–550, https://doi.org/10.1108/RPJ-10-2015-0141.

158. Y. Li, S. Li, X. Du, et al., "A Novel Semi-Flexible Coaxial Nozzle Based on Fluid Dynamics Effects and its Self-Centering Performance Study," *Scientific Reports* 14 (2024): 15606, https://doi.org/10.1038/s41598-024-66623-8.

159. B. Howard, N. D. Wilson, S. M. Newman, C. S. Pfeifer, and J. W. Stansbury, "Relationships Between Conversion, Temperature and Optical Properties During Composite Photopolymerization," *Acta Biomaterialia* 6 (2010): 2053–2059, https://doi.org/10.1016/j.actbio.2009.11.006.

160. S. Farsiani, F. D. Blum, D. N. McIlroy, and H. Noori, "From Light to Kinetics: Studying the Optics of Radical Photopolymerization Evolution," *ACS Applied Polymer Materials* 7 (2025): 11777–11786, https://doi.org/10.1021/acsapm.5c02250.

161. N. C. Brown, D. C. Ames, and J. Mueller, "Multimaterial Extrusion 3D Printing Printheads," *Nature Reviews Materials* 10 (2025): 807–825.

162. J. Stieghorst and T. Doll, "Rheological Behavior of PDMS Silicone Rubber for 3D Printing of Medical Implants," *Additive Manufacturing* 24 (2018): 217–223, https://doi.org/10.1016/j.addma.2018.10.004.

163. N. Rodriguez, S. Ruelas, J.-B. Forien, et al., "3D Printing of High Viscosity Reinforced Silicone Elastomers," *Polymers* 13 (2021): 2239, https://doi.org/10.3390/polym13142239.

164. K. Studer, C. Decker, E. Beck, and R. Schwalm, "Overcoming Oxygen Inhibition in UV-Curing of Acrylate Coatings by Carbon Dioxide Inerting, Part I," *Progress in Organic Coatings* 48 (2003): 92–100, https://doi.org/10.1016/S0300-9440(03)00120-6.

165. M. I. Calafel, M. Criado-Gonzalez, R. Aguirresarobe, M. Fernández, and C. Mijangos, "From Rheological Concepts to Additive Manufacturing Assessment of Hydrogel-Based Materials for Advanced Bioprinting Applications," *Materials Advances* 6 (2025): 4566–4597, https://doi.org/10.1039/D5MA00019J.

166. A. P. Golhin, R. Tonello, J. R. Frisvad, S. Grammatikos, and A. Strandlie, "Surface Roughness of As-Printed Polymers: A Comprehensive Review," *The International Journal of Advanced Manufacturing Technology* 127 (2023): 987–1043, https://doi.org/10.1007/s00170-023-11566-z.

167. A. Hammer, W. Roland, M. Zacher, et al., "In Situ Detection of Interfacial Flow Instabilities in Polymer Co-Extrusion Using Optical Coherence Tomography and Ultrasonic Techniques," *Polymers* 13 (2021): 2880, https://doi.org/10.3390/polym13172880.

168. J. Li, V. Slesarenko, P. I. Galich, and S. Rudykh, "Instabilities and Pattern Formations in 3D-Printed Deformable Fiber Composites," *Composites Part B: Engineering* 148 (2018): 114–122, https://doi.org/10.1016/j.compositesb.2018.04.049.

169. J. O. Hardin, T. J. Ober, A. D. Valentine, and J. A. Lewis, "Microfluidic Printheads for Multimaterial 3D Printing of Viscoelastic Inks," *Advanced Materials* 27 (2015): 3279–3284, https://doi.org/10.1002/adma.201500222.

170. D. C. Ames, S. Propst, A. Shah, and J. Mueller, "Voxel Interface Control in Multimaterial Extrusion 3D Printing," *Advanced Materials* 36 (2024): 2407599, https://doi.org/10.1002/adma.202407599.

171. J. Chen, H. Wen, G. Zhang, et al., "Multifunctional Conductive Hydrogel/Thermochromic Elastomer Hybrid Fibers With a Core–Shell Segmental Configuration for Wearable Strain and Temperature Sensors," *ACS Applied Materials & Interfaces* 12 (2020): 7565–7574, https://doi.org/10.1021/acsami.9b20612.

172. A. Canales, X. Jia, U. P. Froriep, et al., "Multifunctional Fibers for Simultaneous Optical, Electrical and Chemical Interrogation of Neural Circuits In Vivo," *Nature biotechnology* 33 (2015): 277–284, https://doi.org/10.1038/nbt.3093.